Reviews in Mineralogy & Geochemistry
Vol. 58, pp. 315-350, 2005

Crustal Thermal Processes and the Interpretation of Thermochronometer Data

Todd A. Ehlers
Department of Geological Sciences
University of Michigan
Ann Arbor, Michigan, 48109-1063, U.S.A.
tehlers@umich.edu

INTRODUCTION

Many thermochronology studies focus on extracting the thermal history of a sample using fission-track length distributions and track annealing models (e.g., Ketcham 2005, and references therein). Recent developments in measuring the $^{3}He/^{4}He$ concentration profile across apatite grains (e.g., Shuster and Farley 2005) offer a new approach for quantifying sample cooling histories over a broader range of temperatures with the (U-Th)/He system. The motivation behind calculating thermal histories from thermochronometer data has traditionally been to date events such as the onset of exhumation or fault motion, erosion, or for quantifying hydrocarbon maturation in sedimentary basins. The calculation of thermal histories from thermochronometer data is a routine aspect of most thermochronology studies and produces valuable geologic information.

A relevant question for thermochronology studies is what can be learned from forward modeling crustal thermal fields from principles of heat conduction and advection beyond what is already learned from the thermal history extracted from the data? Forward modeling of crustal thermal fields requires a physically based model for heat transfer in the geologic setting of interest. Specific geologic processes such as magmatism, fault motion, fluid flow, as well as the kinematic, topographic, and erosional evolution of an orogen can significantly influence the thermal history of thermochronometer samples. These processes can be simulated with thermal models and then compared to thermochronometer derived cooling histories and ages. Thus, predicted thermal histories and thermochronometer ages generated under a known set of conditions can be compared to observed thermal histories and ages to quantify the geologic processes associated with sample cooling. To answer the question posed earlier, forward modeling crustal thermal fields allows robust, or at least constrained, interpretations of what geologic events could have occurred to produce an observed suite of thermochronometer ages. Hence, comparison of thermochronometer data with model predicted thermal histories and thermochronometer ages allows quantification of different geologic processes.

What is the state of our knowledge concerning crustal thermal fields and processes? A rich body of geothermics literature exists documenting the present day thermal state of the crust from borehole measurements of thermal gradients and thermophysical properties. Excellent compilations of global heat flow determinations are available (Chapman and Pollack 1975; Pollack and Chapman 1977; Sass et al. 1981; Pollack et al. 1993). The influence of different geologic processes on subsurface temperatures has been quantified in previous studies using analytic and/or numerical solutions to differential equations for heat transfer (e.g., Benfield 1949a,b; Carslaw and Jaeger 1959; Lachenbruch 1968; Lachenbruch and Sass 1978; Chapman 1986; Philpotts 1990; Chapman and Furlong 1992). Analytic, or exact, solutions to differential

1529-6466/05/0058-0012$05.00 DOI: 10.2138/rmg.2005.58.12

equations are abundant in the literature and provide a starting point for quantifying the thermal field of many geologic settings under a simplified set of assumptions. More complicated, and more realistic, treatments of crustal thermal processes have been conducted with numerical solutions using techniques such as the finite difference and finite element methods. Numerical methods have the advantage of quantifying transient subsurface temperatures in two or three dimensions, tectonically and topographically complicated areas, and in regions where material properties are variable. However, the implementation of numerical techniques is more complicated than application of analytic solutions and the ability to simulate more complex situations introduces additional free parameters that may be poorly constrained. Which approach—analytic or numerical—to use and when is not easy to determine and often times more simple analytic solutions are sufficient for quantifying a particular process and interpreting a thermochronometer data set. This chapter emphasizes the use of analytic solutions to evaluate the influence of geologic processes on subsurface thermal fields so that readers can acquire an intuitive sense for how to quantify thermochronometer cooling histories. The application of numerical models to selected problems is also highlighted along with addition references describing these methods.

Much of the geothermics literature pertaining to measurements of the crustal thermal field and/or crustal thermal processes is under-utilized by the thermochronology community when attempting to estimate crustal thermal gradients for calculation of sample exhumation rates. The objectives of this chapter are to provide the reader with an understanding of: (1) natural variability in terrestrial heat flow and the conditions under which different geologic processes such as erosion, sedimentation, faulting, magmatism, and fluid flow influence rock thermal histories; (2) how different analytic solutions can be applied to thermochronometer data to quantify geologic processes; and (3) future directions for quantifying geologic processes with coupled low-temperature thermochronometers and thermal models. The closure temperature concept will be used throughout this chapter to simplify the discussion and highlight the effect of geologic processes on subsurface temperatures. Note, however, that a rigorous interpretation of thermochronometer ages necessitates consideration of sample cooling histories and composition. Detailed discussions of how to calculate cooling rate dependent thermochronometer ages are covered in complementary chapters in this volume (e.g., Ketcham 2005; Dunai 2005; Shuster and Farley 2005; and Harrison et al. 2005).

Finally, the supplemental online software archive for this volume includes software which simulates many of the processes discussed here and calculates cooling rate dependent thermochronometer ages (*http://www.minsocam.org/MSA/RIM*). Matlab programs that calculate some of the equations and figures presented here are also available via this online resource. These programs are provided as learning tools to help readers explore how different aspects of the Earth influence subsurface thermal fields and thermochronometer cooling histories. The appendix to this chapter provides a compilation of thermophysical property measurements (e.g., thermal conductivity, specific heat, radiogenic heat production) of common Earth materials.

NATURAL VARIABILITY IN TERRESTRIAL HEAT FLOW

Surface heat flow is the expression of geothermal processes at depth and the analysis of these data provides insight into the nature of these processes. Over 25,000 global heat flow determinations are currently freely available (Commision 2004). Figure 1a shows a global representation of these data (Pollack et al. 1993). This figure was generated using a 12^{th} order spherical harmonic representation of the data, meaning the data set is smoothed over spatial scales of about 3300 km. On spatial scales of this size (10^3 km) global surface heat flow ranges between ~0 and 350 mWm^{-2}. Low values are associated with cratons, very old oceanic crust, and regions with high sediment accumulation rates. High values are associated with

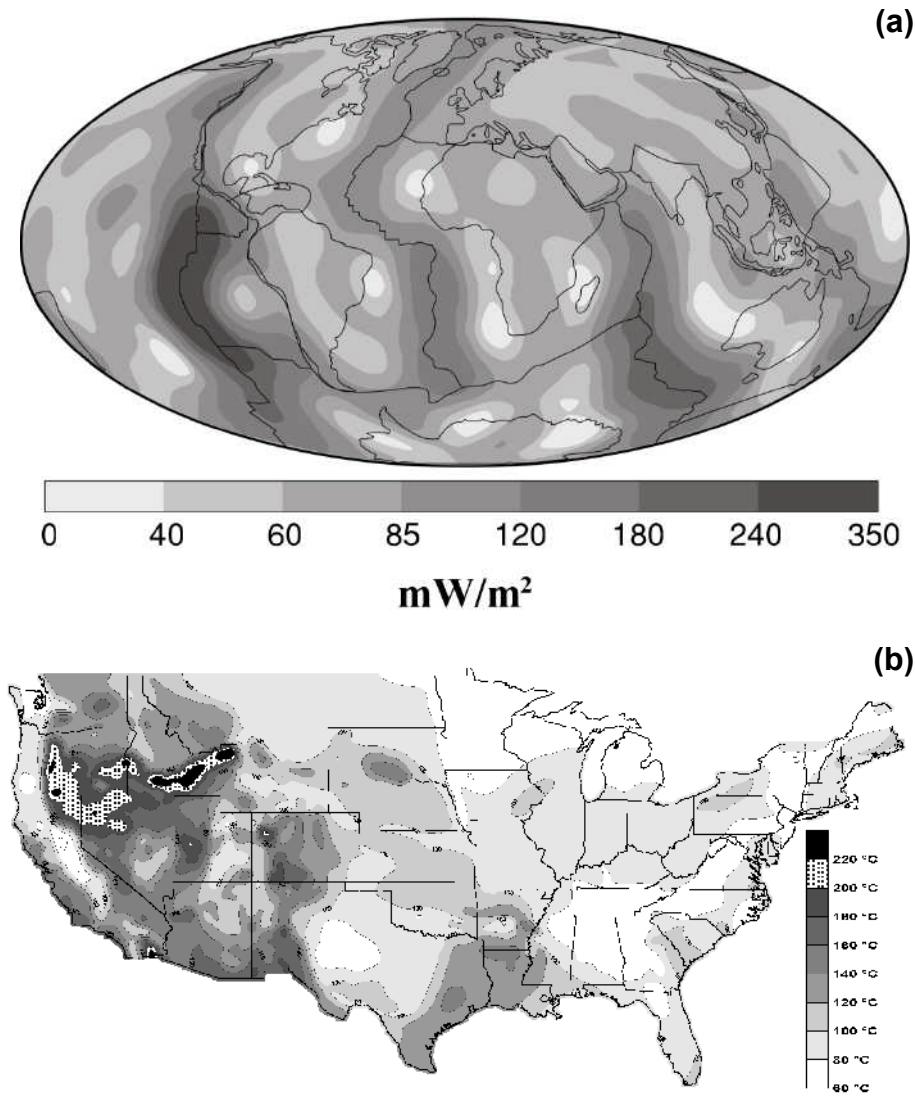

Figure 1. Spatial variations in present day surface heat flow and subsurface temperatures. (a) Long wavelength variations in global heat flow and thermal field contoured with a 12th order spherical harmonic (see text for details). Modified from Pollack et al (1993). (b) Shorter wavelength variations in crustal thermal field for North America. Approximated temperatures at 4 km depth are contoured to highlight spatial variations in subsurface temperatures within individual mountain belts. Modified from Blackwell et al. (1994, 1996).

mid-ocean ridges where new ocean crust is forming. On average terrestrial surface heat flow typically ranges between about 25 and 120 mWm^{-2}. On spatial scales of 10^3 km, variations in terrestrial surface heat flow mimic tectonic provinces (Chapman and Rybach 1985; Furlong and Chapman 1987). Heat flow variations on spatial scales of 10^1–10^2 km (not clearly visible in Fig. 1a) are typically associated with crustal thermal processes such as tectonics, magmatism, or hydrology that affect crustal temperatures. It is on these smaller spatial scales

that thermochronometer data are often collected and awareness to natural variations in surface heat flow and thermal gradients are needed.

Surface heat flow (q) is calculated using Fourier's law such that $q = -kdT/dz$. Parameters in this equation include the measured thermal conductivity of rock (k) and the thermal gradient (dT/dz) measured in a borehole. Thus, thermal gradients and depth to a particular closure temperature can be readily approximated from surface heat flow determinations by dividing the surface heat flow by the thermal conductivity. The thermal conductivity of crustal rocks typically averages around 2.5 $Wm^{-1}k^{-1}$ (see appendix A for details). Dividing the previous range in terrestrial surface heat flow values by this average thermal conductivity provides an estimate of continental variations in thermal gradients. This estimated range in continental thermal gradients is about 10 to 50 °C/km. Thus, significant variation is crustal thermal gradients exist and care must be taken when assuming a thermal gradient to interpret thermochronometer cooling histories. The relevant question at this point is whether or not thermal gradients are significantly variable on the scale of 10^1–10^2 km, the scale at which many thermochronometer sampling campaigns are conducted?

Figure 1b illustrates the variability of thermal gradients in the United States on spatial scales greater than ~ 10^1 km. The figure provides an estimate of temperatures at 4 km depth (Blackwell et al. 1994, 1996). Temperatures at 4 km depth range between 60 and 220 °C, which span the closure temperatures of several thermochronometer systems (e.g., apatite and zircon (U-Th)/He and apatite fission-track data) and highlights a significant natural variability in crustal thermal gradients. A second feature of interest in Figure 1b are the spatial scales over which temperatures vary. For example, individual tectonic provinces (e.g., Rocky Mountain of Colorado, Basin Range of Utah and Nevada, and Sierra Nevada Mountains of Colorado) have significant variations in temperature at 4 km depth on spatial scales of tens of km.

The natural variability in surface heat flow underscores the need to quantify crustal thermal processes when interpreting data sensitive to these variations. A prudent interpretation of thermochronometer data not only considers the present day thermal state of a study area from available heat flow determinations, but also an evaluation of geologic processes influencing the thermal history of thermochronometer data. The remainder of this chapter addresses common geologic processes influencing the thermal history of thermochronometer data.

AGE-ELEVATION PLOTS AND SUBSURFACE TEMPERATURES

A common approach to interpreting thermochronometer data is to plot the sample age versus elevation. This approach is often used because information about the sample exhumation/erosion rate can be inferred from the slope of a best-fitting line through the data. However, several important assumptions about the thermal state of crust underlie the interpretation of exhumation rates from age-elevation plots and care must be taken when applying this technique. The most important assumption commonly made is that all samples pass through the closure temperature at the same elevation. The following section discusses settings where this assumption is valid as well as invalid. In settings where samples do not pass through the closure temperature at the same elevation more sophisticated modeling techniques are required to interpret exhumation rates.

Figure 2 illustrates end-member thermal models associated with the interpretation of thermochronometer data from age-elevation plots (Stuwe et al. 1994; Mancktelow and Grasemann 1997). One end-member model, the horizontal isotherm model (Fig. 2a), assumes the closure isotherm is located at a constant elevation (with respect to sea level) and that samples collected at the surface passed through the closure temperature at the same elevation. In this model, *samples could be collected anywhere across the topography* and, as discussed

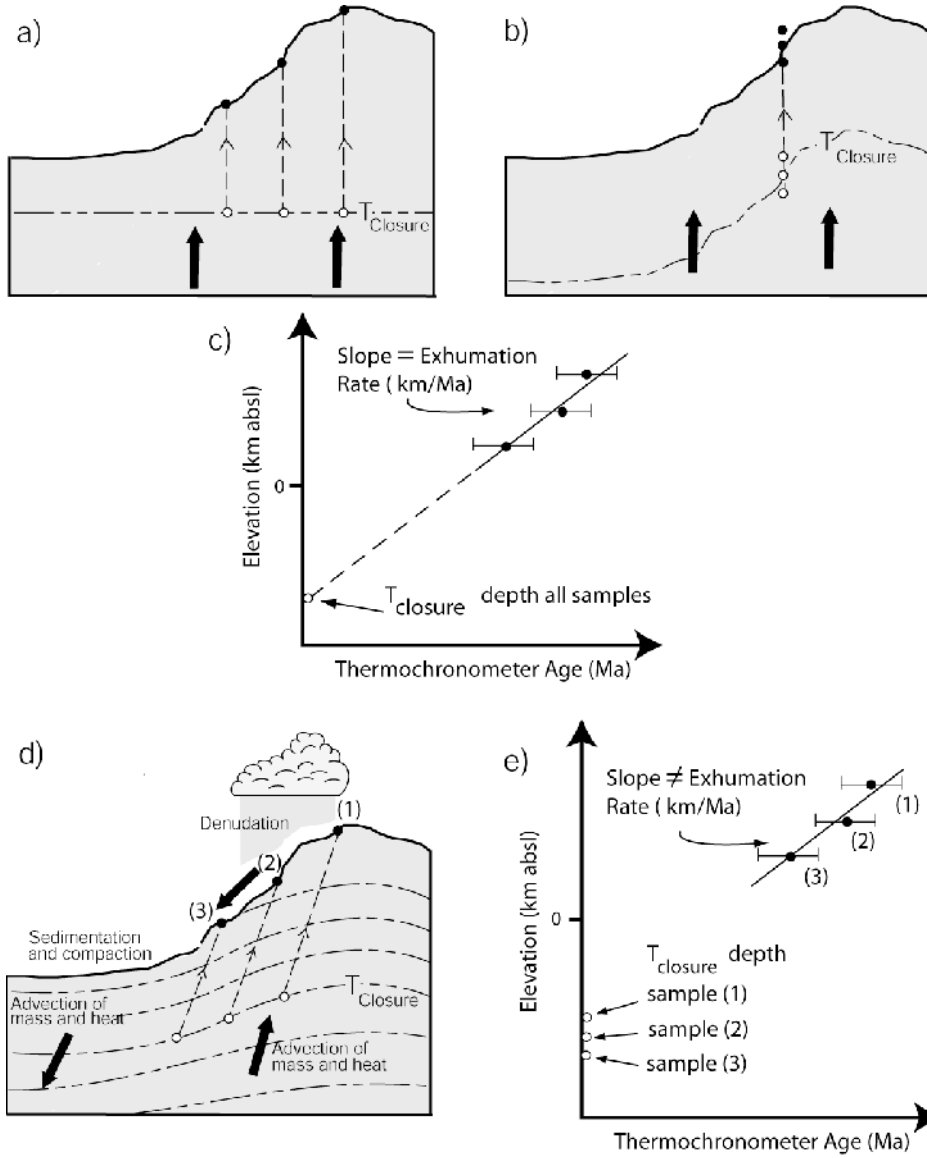

Figure 2. Implication of assumed thermal model on the interpretation of thermochronometer data in age-elevation plots. (a) 1D, horizontal isotherm, thermal model with samples (black circles) collected up a range front. (b) 1D, draped isotherm, thermal model with samples collect up a vertical cliff face. (c) Schematic plot of thermochronometer sample age vs. elevation for the thermal models depicted in (a) and (b). Slope of best fit line equals the sample exhumation rate and depth to closure temperature equals the y-intercept value. (d) Schematic 2D thermal model with variable thermal gradients across range front due to processes illustrated. Each exhumed sample (black circles) pass through the closure temperature at different depths and travel different distances to the surface before exposure. (e) Schematic plot of thermochronometer sample age vs elevation for thermal model shown in (d). Closure depth for each sample is variable and slope of best-fit line through sample ages does not represent the exhumation rate.

below, used to interpret an exhumation rate from a age-elevation plot. This model is applicable for interpreting low-temperature thermochronometer data (e.g., apatite (U-Th)/He or apatite fission track data) in regions with short wavelength (< ~10 km) topography and low erosion rates (e.g., see Stuwe et al. 1994 and Braun 2005 for complete discussion). Alternatively, if higher temperature thermochronometer systems (e.g., biotite, muscovite $^{40}Ar/^{39}Ar$ cooling ages) are being used then this model is also potentially applicable because closure temperature depths are larger and less sensitive to topography (e.g., Stock and Montgomery 1996).

The second end-member model (Fig. 2b) assumes closure isotherms mimic topography. This model assumes the closure temperature is located at a constant depth below the surface, rather than a constant elevation as in the previous case. In this model, *samples should be collected in a purely vertical profile* (e.g., from a cliff face or borehole as shown, Fig. 2b) and would have passed through the closure temperature at the same depth. Geologic settings where this model is relevant include locations where low-temperature thermochronometers (e.g., apatite (U-Th)/He and AFT) with low closure temperatures are investigated, erosion rates are high, and/or long-wavelength (> 40 km) topography is present.

In the previous end-member models the samples in each model pass through the closure temperature at a constant elevation (Fig. 2a) or constant depth (Fig. 2b). Both of these models and sampling strategies represent situations where meaningful information can be interpreted from a plot of the sample age versus elevation. Figure 2c illustrates how an exhumation rate can be calculated from samples if they are plotted in age-elevation space. For example, in both end-member models all the samples pass through the closure temperature at a constant elevation (open circle) and are collected at different elevations on the surface (filled circles). If the assumed thermal model is correct, then a best-fit line through the data should have a y-intercept corresponding to the elevation of the closure temperature and the slope of such a line yields the exhumation/erosion rate. This approach is called the altitude-dependence method (Mancktelow and Grasemann 1997). In practice, these end-member thermal models are not always common and care must be taken before assuming a particular closure isotherm geometry.

Deficiencies in the previous models are several fold and a more realistic model is depicted in Figure 2d where the depth to the closure isotherm and thermal gradients are spatially variable. Thermo-tectonic processes which affect the depth of the closure isotherm include: (1) lateral heat flow across large, range-bounding faults, (2) uplift and erosion, (3) sedimentation and burial, (4) lateral heat refraction around low thermal conductivity sediments deposited in a range front basin, (5) 3D temperature variations due to high-relief topography, (6) magmatism coeval with sample exhumation, (7) topographically driven fluid flow from range crests to valley bottoms, and (8) changes in surface temperature due to the atmospheric adiabatic lapse rate. Low-temperature thermochronometers are sensitive to these thermo-tectonic processes and, as shown in the remainder of this chapter, significant errors can result in calculated exhumation rates due to oversimplified thermal model assumptions such as the examples shown in Figure 2a,b (Grasemann and Mancktelow 1993; Mancktelow and Grasemann 1997; Gleadow and Brown 2000).

Figure 2e illustrates the implication of a non-constant closure temperature depth for samples collected across an orogen as illustrated in Figure 2d. For each of the samples shown in Figure 2e the depth at which the samples passed through the closure temperature is variable because thermal gradients across the range are spatially variable. The sample collected from the highest elevation (sample 1) passed through the closure temperature at a higher elevation than the sample collected at the lowest elevation (sample 3). The implication of variable closure temperature depths is that, unlike previous examples (Fig. 2a,b), there is no physical basis for interpreting an exhumation rate from these samples by taking the slope of a best-fit line through the data because each sample has had a different cooling history.

A more rigorous interpretation of thermochronometer data requires an assessment of the degree to which sample cooling histories depart from the scenarios depicted in Figure 2a,b. Transient and 2D and 3D perturbations to the thermal field can often influence sample cooling ages and result in the situation depicted in Figure 2d,e. Determining if sample cooling histories can be accurately quantified using a 1D constant thermal gradient requires a stepwise evaluation of 2D, 3D, and transient thermal processes using analytic solutions for heat transfer and, if warranted, numerical models. The remainder of this chapter discusses different geologic processes that influence thermochronometer cooling ages and methods to quantify the potential effect of these processes on subsurface temperatures.

GEOLOGIC PROCESSES INFLUENCING THERMOCHRONOMETER AGES

The thermal field of continental crust is influenced by geologic processes that are active on different spatial and temporal scales. For example, sedimentary basin formation occurs on spatial scales of 10^1–10^3 km and although basin infilling in some cases may only occur over 10–20 Ma thermal equilibrium of the crust can take significantly longer and up to 50 Ma or longer. This example highlights the need to quantify the spatial and temporal scale over which the thermal effects of different geologic processes occur and the impact these processes can have on rock thermal histories. In the following section examples of the influence various geologic processes have on the thermal history of thermochronometer samples is discussed.

Background thermal state of the crust

Both conductive and advective heat transfer can be prominent in determining the distribution of temperatures within the crust. Advective heat transfer and spatial variations in heat flow are prevalent in tectonically active areas where mass redistribution by erosion, sedimentation, and fluid flow is common (Blackwell et al. 1989). Conductive heat transfer is more typical of tectonically stable areas and is the starting point for this discussion on the variability of continental geotherms.

The background conductive thermal state of the crust depends on the thermal conductivity, distribution of heat producing radioactive elements, and heat flow into the base of the crust. Prediction of crustal geotherms for different observed surface heat flows is possible using the partial differential equation for time-dependent conductive heat transfer (Carslaw and Jaeger 1959):

$$-div(-k\nabla T) + A = \rho c \frac{\partial T}{\partial t} \tag{1}$$

Where T is temperature, t is time, k is thermal conductivity, A is volumetric heat production and ρ and c are the density and specific heat, respectively. The simplest approach for calculating a crustal geotherm is to consider the case of one-dimensional heat transfer in a homogeneous and isotropic medium with radiogenic heat production. In this case, Equation (1) can be expressed as:

$$\frac{\partial^2 T}{\partial z^2} + \frac{A}{k} = \frac{1}{\alpha}\frac{\partial T}{\partial t} \tag{2}$$

where α is the thermal diffusivity and defined by $\alpha = k/\rho c$. Further simplification of this equation to steady-state heat transfer produces the ordinary differential equation known as Poisson's equation:

$$\frac{d^2 T}{\partial z^2} = -\frac{A}{k} \tag{3}$$

The solution to Poisson's equation in 1D is:

$$T(z) = T_0 + \frac{q_0}{k} z - \frac{Az^2}{2k} \quad (4)$$

Where T_0 and q_0 are the temperature and heat flow at Earth's surface, respectively.

The final step required for calculating steady-state geotherms is assignment of material properties such as thermal conductivity and heat production. Thermal conductivity is primarily determined by composition, but also influenced by temperature and pressure (Cermak and Rybach 1982). Thermal conductivity of common crustal rocks ranges between 1.5 (shale) and 6.0 (quartz arenite) $Wm^{-1}K^{-1}$. A value of 3.0 $Wm^{-1}K^{-1}$ is used here and is an appropriate average value for upper crustal rocks (Roy et al. 1981, see also appendix A). Radiogenic heat production is highly variable in the upper crust and ranges between 0.3 (basalt) to 2.5 (granite/rhyolite) μWm^{-3}, with an average continental crust value of 0.8 μWm^{-3} (Taylor and McLennan 1981; Ryback and Cermak 1982, see also appendix A). The distribution of heat production in the crust varies both laterally and with depth, thereby significantly influencing subsurface temperatures (Pollack 1982). For the upper crust, an exponential decreasing heat production is used such that:

$$A(z) = A_0 \exp\left(\frac{-z}{D}\right) \quad (5)$$

where A_0 is the surface heat generation, z is depth, and D is the characteristic depth over which heat producing elements are distributed. Average crustal values of A_0 and D are 2.0 μWm^{-3} and 10 km, respectively.

Figure 3 shows a suite of steady-state continental geotherms calculated for surface heat flow variations between 40 and 90 mWm^{-2}. The geotherms were calculated using Equations (4) and (5), and the interval method of (Chapman 1986). The geotherms illustrate how subsurface temperatures and thermal gradients vary for a range in terrestrial heat flow. The most important aspect of this figure is the divergence of temperatures with depth from the common surface temperature of 0 °C. For example, at 20 km depth (Fig. 3a) temperatures vary from 220 °C for the 40 mWm^{-2} geotherm to 475 °C for the 90 mWm^{-2} geotherm. A more subtle aspect of each geotherm is the slight downward curvature. The curvature of geotherms is due to heat production and the decrease of heat producing elements with depth (Eqn. 5).

Variation in the depth at which a particular temperature occurs can influence the interpretation of thermochronometer cooling ages. For example, apatite (U-Th)/He and apatite fission-track (AFT) samples are sensitive to the thermal history between 50–90 °C, and 90–150 °C, respectively. Using the 100 °C isotherm for reference, Figure 3b suggests the depth of this isotherm ranges between ~3.4 and 8.2 km for surface heat flow between 90 and 40 mWm^{-2}, respectively. The corresponding average thermal gradients over these depths are 30 and 12 °C/km for the same range in surface heat flow. This variation in thermal gradients is significant because many thermochronometer studies use an average crustal thermal gradient of ~25 °C/km to calculate a depth to closure and an exhumation or burial rate. The point emphasized here is that terrestrial surface heat flow is variable around the world (Fig. 1a), and even within individual orogens (Fig. 1b). Therefore, the notion that exhumation and burial rates can be calculated from an average continental thermal gradient must be discarded. The natural variability in thermal gradients is large enough that significant errors can be introduced into exhumation rate calculations.

Equation (4) provides the basis for calculating the background thermal state of the crust. The thermal consequence of the other geologic processes discussed below are all superimposed upon the heat transfer processes and concepts illustrated in this section. Using

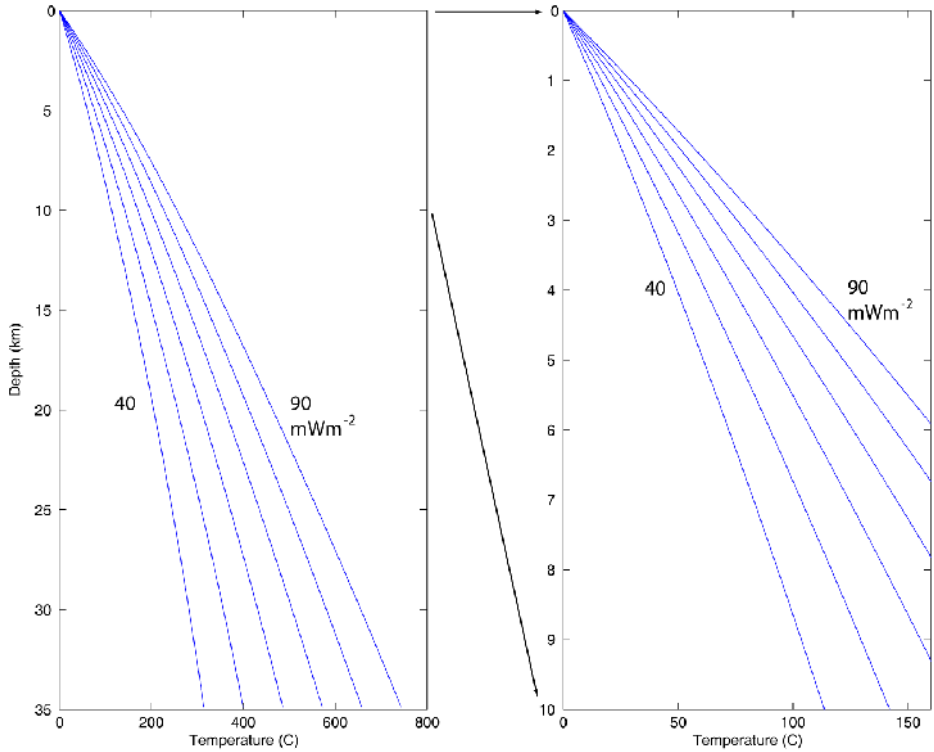

Figure 3. Steady-state crustal geotherms calculated as a function of surface heat flow. Geotherms were calculated for surface heat flow values of 40, 50, 60, 70, 80, and 90 mWm^{-2} using Equation (4). Material properties used include a constant thermal conductivity of 3.0 $Wm^{-1}k^{-1}$ and variable heat production with depth (Eqn. 5) assuming A_o = 2.0 uWm^{-3} and D = 10 km. A Matlab program that reproduces Figure 3 is provided in the supplemental software archive.

thermochronometers to interpret thermal histories from geotherms predicted by Equation (4) should be done only in tectonically stable areas with very slow erosion or sedimentation and minimal topographic influence at closure temperature depths.

Erosion and sedimentation

Significant interest has emerged in the last decade to quantify rates of landscape evolution using low-temperature thermochronometry (House et al. 1998; House et al. 2001; Braun 2002; Persono et al. 2002; Ehlers and Farley 2003). Thermochronometer data are particularly well suited to quantify the rates of landscape and sedimentary basin evolution over million year timescales, which is a timescale where other geochronology techniques (e.g., cosmogenic ^{10}Be, ^{26}Al nuclides) start to lose sensitivity to these processes. Landscape evolution results in the redistribution of mass through the processes of erosion and sedimentation. The redistribution of mass by these processes also results in the redistribution of heat. For example, erosion removes material from Earth's surface resulting in the upward movement of warmer rocks. This upward movement of rocks causes a net increase in temperature at any given depth relative to the initial temperature prior to erosion. Sedimentation can have the opposite effect on subsurface temperatures. As sediment is deposited on the surface of Earth the cool surface temperature is advected downward, thereby causing a net decrease in temperatures at any depth below the surface relative to temperatures prior to sedimentation. If erosion and

sedimentation occur at sufficiently high rates (i.e., > ~0.1–0.2 mm/yr) then heat transfer is no longer purely by conduction and advective transfer can be important.

One caveat related to material properties needs mention here, namely that thermal gradients in sedimentary basins can also increase if the density and thermal conductivity of the sediment are sufficiently low. Although the following discussion does not quantify this effect, realize that advection of mass by sedimentation decreases thermal gradients whereas the material properties of the sediment deposited can sometimes increase the gradients. Thus, the effect of these two processes on thermal gradients are opposite in direction.

Calculation of subsurface temperatures. The previously discussed thermal effects of erosion and sedimentation on subsurface temperatures can be quantified with the transient advection-diffusion partial differential equation. Application of the advection-diffusion equation to problems in landform evolution typically requires a 2D or 3D form of the equation to quantify rates and magnitudes of topographic change (e.g., Stuwe et al. 1994; Mancktelow and Grasemann 1997). The 1D form of the advection-diffusion equation will be discussed here to illustrate the physical consequences of sedimentation and erosion on subsurface temperatures, and more complicated 2D solutions will be discussed later. In 1D with no heat production, the advection-diffusion equation is given by (Carslaw and Jaeger 1959):

$$\alpha \frac{\partial^2 T}{\partial z^2} = \frac{\partial T}{\partial t} + v \frac{\partial T}{\partial z} \tag{6}$$

where α is the thermal diffusivity, T is temperature, t is time, z is depth, and v is the velocity of the medium relative to Earth's surface. If z is defined in a coordinate system such that it is positive downward into Earth, then a negative value of v represents erosion and a positive value of v represents sedimentation. In Equation (6), the left-hand term describes conductive heat transfer, the middle term transient heat transfer, and the right hand term advective heat transfer by erosion or sedimentation.

Equation (6) can be solved by assuming a constant surface temperature (T_0) at $t = 0$, $z = 0$ and equilibrium initial thermal gradient (Γ_b) prior to erosion or sedimentation at time $t = 0$. The solution for transient subsurface temperature is then (Powell et al. 1988):

$$T(z,t) = T_0 + \Gamma_b (z - vt) + \frac{1}{2}\Gamma_b \times \left[(z + vt) \exp\left(\frac{vz}{\alpha}\right) erfc\left(\frac{z + vt}{2(\alpha t)^{\frac{1}{2}}}\right) - (z - vt)\, erfc\left(\frac{z - vt}{2(\alpha t)^{\frac{1}{2}}}\right) \right] \tag{7}$$

where all variables are the same as before and *erfc* is the complementary error function (Abramowitz and Stegun 1970). Equation (7) is an appropriate starting point for understanding the effect of sedimentation and erosion of subsurface temperatures.

Figure 4 shows a set of transient crustal geotherms calculated using Equation (7). These geotherms were calculated assuming a constant sedimentation or erosion rate of 1 mm/yr. For the case of sedimentation (Fig. 4a), subsurface temperatures at any depth get cooler from their initial temperature as the duration of sedimentation increases. For example, at 4 km depth (Fig. 4a) the initial temperature ($t = 0$) is 100 °C. After 5, 10, and 15 Ma of sedimentation at 1 mm/yr the temperature at 4 km depth decreases to 70, 55, and 46 °C, respectively. Note from this example that the rate of temperature change decreases with time such that between 0 and 5 Ma the temperature at 4 km depth changes 30 °C per 5 Ma, whereas between 5-10 Ma and 10-15 Ma the temperature change is 15 and 9 °C per 5 Ma, respectively. This decrease in temperature change with time is a result of the thermal field approaching steady-state.

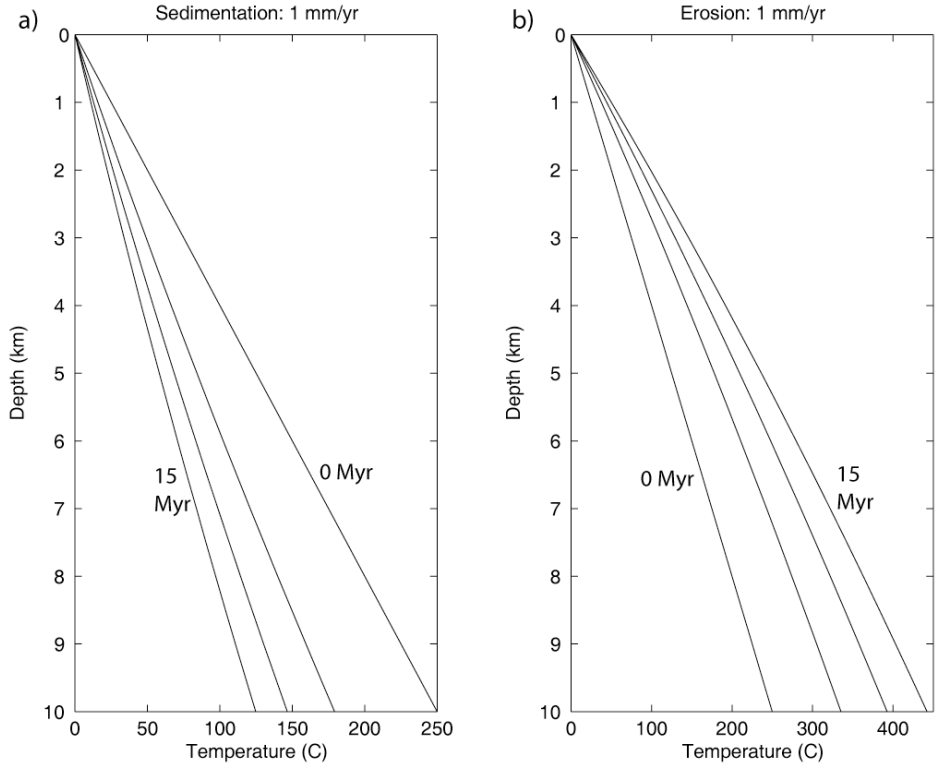

Figure 4. Transient crustal geotherms calculated as a function of erosion and sedimentation. Prescribed erosion and sedimentation rates are 1 mm/yr, with geotherms shown after 0 (initial condition), 5, 10, and 15 Ma of erosion or sedimentation. (a) Influence of sedimentation on geotherms. (b) Influence of erosion on geotherms. Results were calculated using Equation (7) and the following parameters, surface temperature of 0 °C, initial thermal gradient of 25 °C/km, and thermal diffusivity of 32 km^2Ma^{-1}. A Matlab program that reproduces Figure 4 is provided in the supplemental software archive.

The thermal effect of sedimentation decreasing subsurface temperatures must be taken into account when interpreting thermochronometer data collected from sedimentary basins (e.g., Armstrong and Chapman 1999).

Erosion has the opposite effect on subsurface temperatures than sedimentation and rock temperatures at a particular depth increase relative to their initial temperature. For example, in Figure 4b after 5, 10, and 15 Ma of erosion temperatures at 4 km depth increase from 100 °C (at $t = 0$) to 140, 170, and 195 °C, respectively. Thus, upper crustal temperatures progressively increase, and thermal gradients are enhanced in response to erosion. The magnitudes of temperature change between the time intervals of 0–5, 5–10, and 10–15 Ma are 40, 30, and 15 °C per 5 Ma. Note that, as with the case of sedimentation, the magnitude of temperature change decreases with time but that with erosion the change is larger. For example, between 0–5 Ma temperatures at 4 km depth change by 30 °C during sedimentation and 40 °C for erosion. The larger magnitude of temperature change due to erosion compared to sedimentation is a consequence of the direction material is moving with respect to the boundary conditions used to solve Equation (6). For sedimentation, material is moving downward and away from a constant surface temperature, thereby advecting heat downward. For erosion, material is moving upward and away from a constant gradient boundary condition where temperature is

free to increase as long as the gradient stays constant, thereby resulting in a larger magnitude of temperature change. The warming of temperatures at depth and enhanced thermal gradients due to erosion must be taken into account in exhumation and erosion studies in active orogenic settings as rocks cool along their trajectory to the surface.

Thermal gradient perturbations. A common problem encountered by Earth scientists working with thermochronometer data is knowing when a process such as erosion or sedimentation has occurred at a high enough rate and for long enough time to influence their interpretation of data. For example, the interpretation of exhumation rates from age-elevation plots (e.g., Fig. 2a,b) assumes thermochronometer samples cool through a temporally and spatially constant thermal gradient. However, in settings where erosion rates are low and/or erosion durations short the perturbation to thermal gradients at closure temperature depths can be negligible. Furthermore, quantifying changes in thermal gradients as a function of an erosion or sedimentation rate is important to understanding how the cooling rate of samples changes. Changes in a cooling rate (dT/dt) are proportional to the product of the thermal gradient (dT/dz) and the erosion or sedimentation rate (dz/dt), where T is temperature, z is depth, and t is time. Thus, quantifying changes in thermal gradients is a necessary step to quantifying changes in cooling rates and calculation of cooling rate dependent closure temperatures (e.g., Dodson 1973,1986; Farley 2000). The following discussion highlights a 1D approach to quantifying first order effects of erosion and sedimentation on thermal gradients and cooling rates.

The previous 1D advection-diffusion Equation (6) can be used to estimate the influence of erosion and sedimentation on crustal thermal gradients. The solution of Equation (6) for corresponding gradients is given by (Benfield 1949b; Kappelmeyer and Haenel 1974; Powell et al. 1988):

$$\frac{\partial T(z,t)}{\partial z} = \Gamma_b + \frac{1}{2}\Gamma_b \bullet \left[-erfc\left(\frac{z - vt}{2(\alpha t)^{\frac{1}{2}}} \right) - \frac{z + vt}{(\pi \alpha t)^{\frac{1}{2}}} \exp\left(\frac{vz}{\alpha} \right) \exp\left(-\left(\frac{z + vt}{2(\alpha t)^{\frac{1}{2}}} \right)^2 \right) \right.$$
$$\left. + \frac{z - vt}{(\pi \alpha t)^{\frac{1}{2}}} \exp\left(-\left(\frac{z - vt}{2(\alpha t)^{\frac{1}{2}}} \right)^2 \right) + \left(1 + \frac{vz}{\alpha} + \frac{v^2 t}{\alpha} \right) \exp\left(\frac{vz}{\alpha} \right) erfc\left(\frac{z + vt}{2(\alpha t)^{\frac{1}{2}}} \right)^2 \right] \quad (8)$$

Equation (8) can be used to quantify the effect of sedimentation and erosion on thermal gradients at Earth's surface and at the depths and temperatures sensitive to low-temperature thermochronometers. Figure 5 uses Equation (8) to calculate thermal gradient changes as a function of different erosion/sedimentation rates and durations. The parameters assumed for making Figure 5 are identical to those used in Figure 4, including the initial thermal gradient (Γ_b = 25 °C/km). On typical time-scales of orogenic development (10^6–10^7 years) thermal gradients at Earth's surface can significantly change from their initial value at erosion and sedimentation rates greater than ~0.1 mm/yr (Fig. 5a,b). For example, at a sedimentation rate of 1 mm/yr (Fig. 5a) the initial thermal gradient of 25 °C/km remains unaffected until about 10^3 years, at which time the gradient starts to decrease. After 10^6 and 10^7 years of sedimentation at the same rate the thermal gradient will decrease to 20 and ~12 °C/km, respectively. Erosion has the opposite effect (Fig. 5b) and causes an increase in thermal gradients with increased erosion duration. Figure 5a,b also clearly shows that the disturbance to thermal gradients from an initial value is more pronounced at higher rates. For example, after 10^5 years of erosion at 10 mm/yr the thermal gradient doubles from 25 to 50 °C/km (Fig. 5b). Thus, the magnitude of change in thermal gradients within active orogenic settings is highly sensitive to both the rate and duration of sedimentation or erosion. Furthermore, the previous discussion highlights

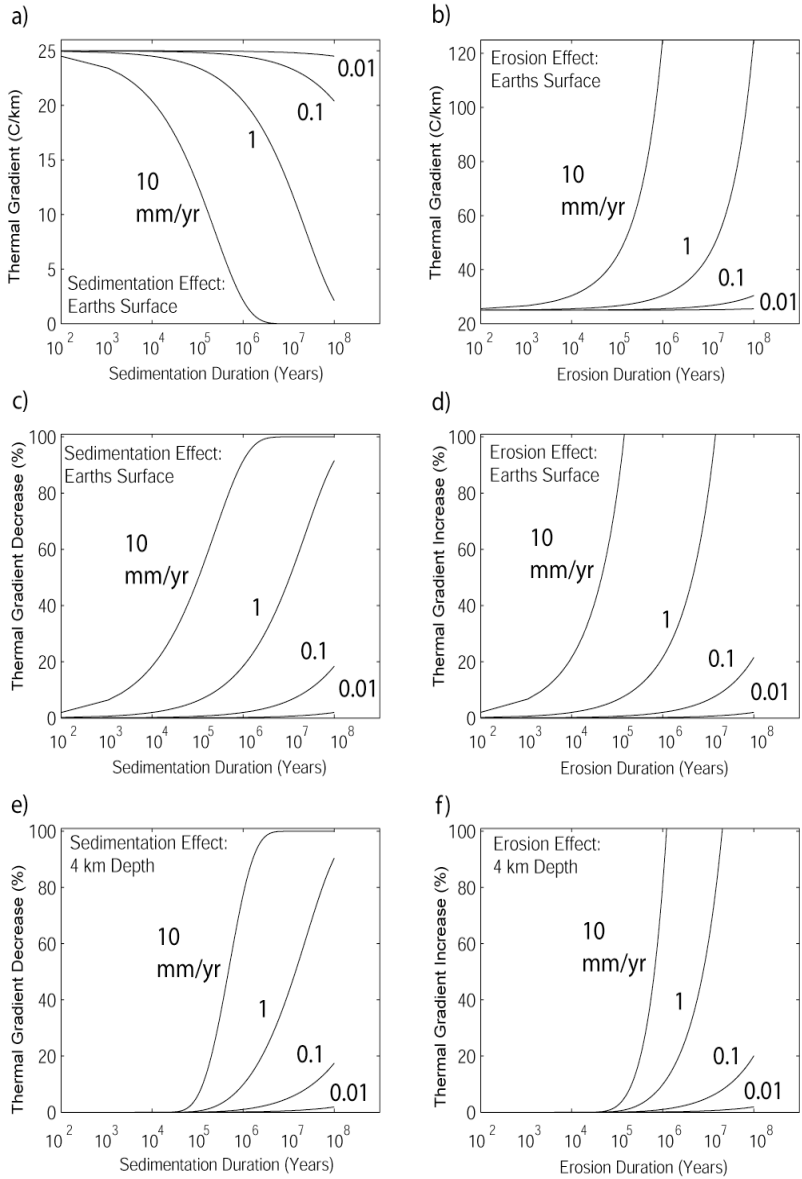

Figure 5. The effect of erosion and sedimentation rate and duration on thermal gradients. Affect of sedimentation (a) and erosion (b) on thermal gradients at Earth's surface for an initial thermal gradient of 25 °C/km. Generalized % effect of sedimentation (c) and erosion (d) on thermal gradients at Earth's surface. Effect of sedimentation (e) and erosion (f) on thermal gradients at 4 km depth. All results were calculated using Equation (8) and the same parameters as in Figure 4. Percent gradient increase or decrease (y-axis) in (c) thru (f) was calculated as percent effect with respect to the initial thermal gradient prior to onset of erosion or sedimentation. The calculated % increase or decrease is applicable to any initial thermal gradient. A Matlab program that reproduces Figure 5 is provided in the supplemental software archive.

the transient evolution of thermal gradients and draws into question assumptions of constant cooling rates often used to interpret thermochronometer data (e.g., Fig. 2).

Present day near surface thermal gradients are spatially variable (e.g., Fig. 1). The remainder of this section generalizes the results of Figure 5a,b, which assumed an initial thermal gradient of 25 °C/km, to show how erosion and sedimentation influence thermal gradients for any initial thermal gradient. Figure 5c-f use Equation (8) to show the *percent thermal gradient change relative to any initial thermal gradient* (Γ_b) as a function of erosion and sedimentation duration and rate. At Earth's surface (Fig. 5c,d) the effect of sedimentation and erosion on thermal gradients increases with the duration of activity and with the rate at which the process occurs. For example, after 1 Ma ($t = 10^6$ years) of sedimentation the thermal gradient is decreased by ~3%, 20%, and 90% for rates of 0.1, 1.0, and 10 mm/yr, respectively (Fig. 5a). After 1 Ma of erosion (Fig. 5d) the thermal gradient is perturbed 5%, 30%, and 200% (not shown) at rates of 0.1, 1.0, and 10 mm/yr. The magnitude of gradient perturbation is greater for erosion than sedimentation because of the direction material is moving with respect to boundary conditions as previously discussed.

At depths around 4 km where low-temperature thermochronometer data such as apatite (U-Th)/He or fission-track are at or near closure, thermal gradients are also influenced by the processes of sedimentation and erosion (Fig. 5e,f). The magnitude of perturbation these processes have on thermal gradients is comparable to those previously discussed. However, at 4 km depth the gradient perturbation is delayed from the time at which it occurs at the surface. For example, for a sedimentation rate of 1 mm/yr, perturbation to the thermal gradient at the Earth's surface starts at ~1,000 years (Fig. 5a) after the onset of sedimentation whereas at 4 km depth an effect is not noticed until ~100,000 years (Fig. 5e). A similar delay in gradient perturbation occurs for the case of erosion (compare Fig. 5d and 5f). The time delay in thermal gradient perturbations at depth is due to the extra time it takes processes occurring at Earth's surface to penetrate downward. The primary controlling factors on the magnitude of the time delay are the rate at which the process is occurring and the thermal diffusivity of the rock.

When taking into account the influence of sedimentation and erosion on thermal gradients and the interpretation of thermochronometer data it is important to not only consider the rate but also the time span over which the sedimentary basin or orogen has been evolving. Figure 5 provides a means to quickly assess the impact of these processes on, for example, the calculation of sedimentation or erosion rates. If erosion or sedimentation rates in a study area are estimated from other geologic constraints to be <0.1 mm/yr then disturbances to the background thermal field will be less than ~10% for durations on order 10 Ma or less. However, if rates are estimated to be higher or durations longer than perturbations to the background gradient could be significantly larger and a more sophisticated treatment of the data to quantify sedimentation or erosion rates may be warranted.

Tectonics and faulting

Thermochronometer data are often used to quantify the timing and rates of fault motion in orogenic belts. In this section the influence of fault motion on thermochronometer data is discussed and references to more detailed observational and modeling studies are presented. In tectonically active areas several processes influence the cooling history of thermochronometer data and cause departures from the simple 1D background thermal field represented in Equation (4) (Fig. 6). The largest disturbance to the background thermal field typically arises from erosion and sedimentation transporting mass from one side of the fault to the other. In extensional, normal fault bounded, mountain ranges erosion of the footwall causes an enhanced thermal gradient in the footwall (e.g., Fig. 4b, Fig. 6a) whereas sedimentation on the hanging wall results in a depressed thermal gradient (e.g., Fig. 4a). In extensional settings where erosion and sedimentation are minimal and rocks are exposed at the surface by tectonic exhumation in

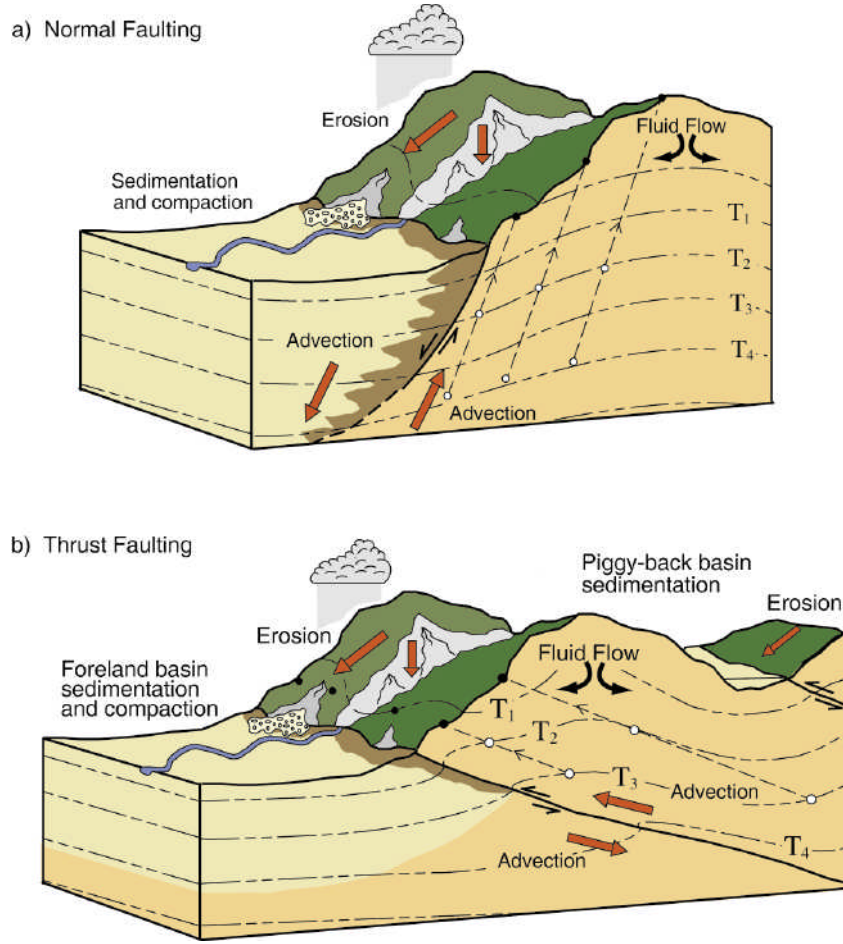

Figure 6. Schematic of thermo-tectonic processes influencing thermochronometer interpretation. (a) Processes influencing thermochronometer interpretation in normal fault settings modified from Ehlers et al (2003). (b) Processes influencing thermochronometer interpretation in thrust tectonic settings modified from Ehlers and Farley (2003). Subsurface isotherms (dashed lines) are indicated with temperatures increasing from T_1 to T_4. Open circles represent position and trajectory of rocks eventually exposed at the surface (filled circles).

the footwall a similarly enhanced footwall thermal gradient can also occur. The reverse effect occurs in compressional, or thrust tectonic, mountain ranges (Fig. 6b) where erosion of the hanging wall enhances thermal gradients and foreland basin sedimentation on the footwall depresses thermal gradients. There are several important thermal consequences to the previous description of mass redistribution across faults (Fig. 6): (1) rates of erosion and sedimentation on each side of the fault can cause significant departures from the background thermal field as discussed in the previous section, (2) the juxtaposition of enhanced and depressed thermal fields across the fault causes lateral heat flow across the fault and curved isotherms at thermochronometer closure temperature depths, and (3) sedimentation and basin formation can result in thermal conductivity contrasts across the fault and lateral heat flow. If the rates of fault motion, erosion, and sedimentation are sufficiently fast (e.g., > ~0.1 mm/yr, Fig. 5d,f) then a

significant contrast in thermal gradients across the fault can violate assumptions of vertical, 1D, heat flow (e.g., Eqns. 4 and 7) and 2D or even 3D heat transfer should be considered.

Several other thermal processes associated with mountain building can result in lateral variations in thermal gradients and multidimensional heat flow. These processes include: (1) frictional heating on faults with slip rates of > ~1 cm/yr (e.g., Lachenbruch and Sass 1980), (2) thickening of radiogenic heat producing layers in thrust tectonic settings, (3) stripping off or removal of high heat producing layers from erosion of the uplifted block, (4) displacement on adjacent or underlying thrusts, (5) topographic development and 3D heat flow in the uplifted block, and (6) topographically driven fluid flow from the uplifted block to the valley floor.

Normal faulting. Several numerical modeling studies have quantified the influence of normal faulting on subsurface temperatures and found normal faulting to significantly influence subsurface temperatures when rates of extension are sufficiently fast enough (Furlong and Londe 1986; Ruppel et al. 1988; van Wees et al. 1992; Bertotti and ter Voorde 1994; ter Voorde and Bertotti 1994; Govers and Wortel 1995; Bertotti et al. 1999; Ehlers and Chapman 1999; Ehlers et al. 2001; Armstrong et al. 2003; Ehlers and Farley 2003). Figure 7 highlights the effect of normal faulting and footwall tilt on the interpretation of thermochronometers in age-elevation plots (Ehlers et al. 2001). Samples collected on a traverse between a fault and range crest (open circles in Fig. 7a) will, among other things, be sensitive to the exhumation rate at the fault and the magnitude of footwall tilt. This type of sampling strategy is useful when trying to determine the timing, rate, magnitude, and structural tilt of normal fault bounded ranges. Synthetic (U-Th)/He and AFT data were simulated for this setting using two fault-adjacent exhumation rates of 1.1 (solid lines) and 0.5 (dashed lines) mm/yr (Fig. 7b), Footwall tilt causes range crest samples (2 km elevation) to exhume at slower rates of ~0.9 and 0.3 mm/yr. The predicted sample age after 10 km of exhumation is shown with the open circles and a 1D thermal model (e.g., Fig. 2a,b) based best-fit line through each data set is shown (V_{1D} values). Note that the 1D thermal model does not account for footwall tilt so only one exhumation rate can be calculated from the data.

Two general trends are visible in the predicted (U-Th)/He and AFT ages (Fig. 7b). First, with an increase in exhumation rate, the difference between (U-Th)/He and AFT ages will decrease. This is evident by comparing the age difference between the two fast and slow exhumation rate pairs of curves. This decrease in age differences with increased exhumation rate is a direct result of material moving faster towards the surface and higher exhumation rates shifting isotherms closer to the surface and decreasing the distance between apatite (U-Th)/He and fission track closure temperatures. A second visible trend in the predicted ages is that for either pair of (U-Th)/He and AFT samples, both exhumed at an identical exhumation rate, the slope of the best fit line through the data is different, with the (U-Th)/He samples having a steeper slope than the AFT samples. A 1D thermal model would yield the incorrect interpretation that the steeper slope of the (U-Th)/He data suggests an increase in the exhumation rate relative to the AFT data. However, the different slopes between each pair of (U-Th)/He and AFT data is a result of an increase in the thermal gradient at shallow (U-Th)/He closure temperature depths and the 2D nature of the thermal field (e.g., Fig. 2d,e).

Differences between the 2D and 1D fault perpendicular exhumation rates are as follows. For samples exhumed at 1.1 mm/yr adjacent to the fault (solid lines in Fig. 7b), the 1D thermal model predicts average (U-Th)/He and AFT exhumation rates of 1.2 and 0.8 mm/yr, respectively. Neither 1D exhumation rate is correct with respect to the simulated exhumation rates (v_{exh}) and errors are between 0.1 and 0.3 mm/yr (~10–30%) compared to the fault-adjacent exhumation rate. The (U-Th)/He and AFT samples exhumed at the slower, fault-adjacent rate of 0.5 mm/yr (dashed lines in Fig. 7b) have predicted 1D exhumation rates of 0.4 and 0.3 mm/yr, respectively. The (U-Th)/He and AFT 2D and 1D exhumation rates differ by 0.1 mm/yr (20%)

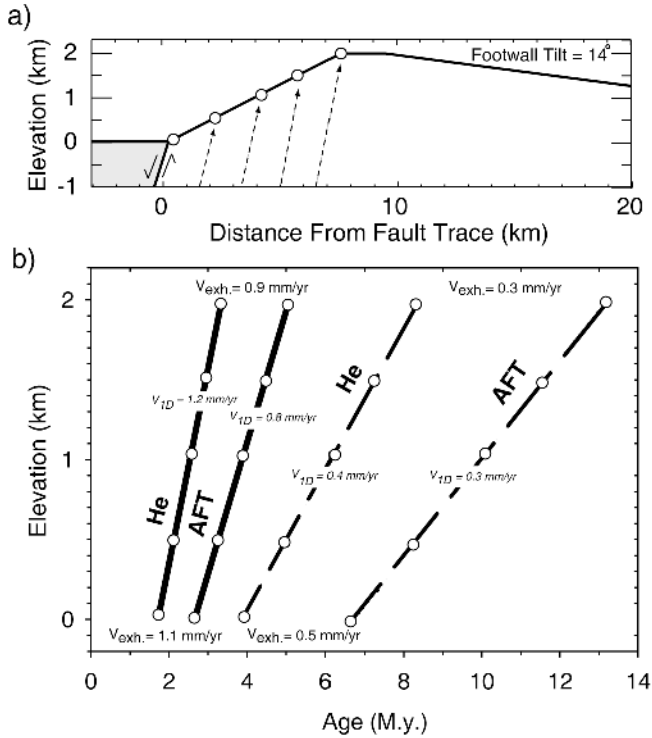

Figure 7. Numerical model predicted sensitivity of interpreted exhumation rates to the assumed thermal model in normal fault bounded ranges. (a) Location of samples collected up the front of a normal fault bounded range. Circles represent sample collection locations, dashed lines represent sample exhumation trajectories. (b) Predicted sample ages (open circles) versus elevation for sample collected along profile shown in (a). The 1D exhumation rates (V_{1D}) refer to rates calculated using the altitude-dependence method (e.g., Figure 2c). The 2D exhumation rates (V_{exh}) refer to the exhumation rate along the samples exhumation trajectory (e.g., Figure 2e). Sample ages in (b) were calculated using a spherical ingrowth diffusion model, and fission-track annealing model for apatite He and apatite fission track ages, respectively (methods described in Ehlers et al. 2004). Modified from Ehlers et al. (2001).

and 0.2 mm/yr (40%), respectively, at the range front. The magnitude of error in 1D exhumation rates generally increases with increased exhumation rate. The difference, or error, between 1D and simulated (v_{exh}) exhumation rates exceed typical uncertainties in measured (U-Th)/He and AFT data and should be of concern when interpreting thermochronometer data.

Thrust faulting. Extensive work has been directed towards delineating the structural evolution of fold and thrust belts (e.g., Suppe 1976, 1980, 1983; Boyer and Elliot 1982; Mitra 1986; Homza and Wallace 1995; Thorbjornsen and Dunne 1997; Martel 1999). Many of these studies have focused on structural styles of deformation and described specific structures such as fault-bend folds, imbricate fans, and duplexes (e.g., Boyer and Elliot 1982; Suppe 1983; Mitra 1986; Allmendinger and Shaw 2000; Salvini et al. 2001) or have described kinematic patterns of structural thickening that occur with underplating (Platt et al. 1985). Large-scale kinematic descriptions of fold and thrust belts reached their apogee with the construction of balanced cross-sections which facilitate the restoration of pre-deformational strata (e.g., Dahlstrom 1969; Jones 1971; Elliott 1976, 1977, 1983; Suppe 1980, 1983; Boyer and Elliot 1982).

Several studies have made significant advances in understanding thrust fault kinematics using apatite fission-track thermochronometry (e.g., Cerveny and Steidtmann 1993; Burtner and Nigrini 1994; Burtner et al. 1994; Omar et al. 1994; O'Sullivan et al. 1998; Quidelleur et al. 1997; Rahn and Grasemann 1999). The focus of most of these studies has been to determine the chronology of thrusting on different faults, exhumation magnitude, and in some cases rates of faulting on a single thrust fault. Most of these studies implement one or more of the following approaches: (1) use one-dimensional (1D) thermal models to deduce exhumation parameters, (2) assume 1D (vertical) kinematics for sample exhumation pathways, (3) ignore sample cooling due to erosion (versus structural cooling and subsequent warming) or prescribed erosion histories, and (4) neglect the 2D thermal, kinematic, and erosional implications that laterally adjacent imbricate or underlying (duplex) thrust faults may have on exhumed thermochronometer sample ages. To the best of my knowledge, no published studies have investigated the thrust belt kinematic processes influencing apatite (U-Th)/He cooling ages.

However, a rich body of literature is available discussing the thermal processes of thrust faulting (e.g., Edman and Surdam 1984; Furlong and Edman 1984, 1989; Edman and Furlong 1987). Studies of individual thrust sheets represent the vast majority of these studies. The simplest of these thermal models consider 1D heat flow through a thrust sheet emplaced instantaneously on top of a relatively cool footwall (e.g., Oxburgh and Turcotte 1974; Graham and England 1976; Brewer 1981; Angevine and Turcotte 1983; Edman and Surdam 1984; England and Thompson 1984; Davy and Gillett 1986; Mailhe et al. 1986; England and Molnar 1993; Husson and Moretti 2002). At the next level of sophistication, 1D models were stacked laterally to approximate 2D heat flow or finite thrust emplacement rates (Karabinos and Ketcham 1988). Fully 2D models were also applied to the thrust-sheet emplacement problem (Shi and Wang 1987; Molnar and England 1990, 1993; Ruppel and Hodges 1994; Quidelleur et al. 1997; Rahn and Grasemann 1999; Husson and Moretti 2002). Recent work by (ter Voorde et al. 2004) has used a 2D thermal model with prescribed erosion histories to investigate the thermal consequence of adjacent thrust faults and thickening of radiogenic heat producing layers. Future work in modeling thrust belt thermal processes is needed to quantify the thermal effects of multiple thrusts, timing and rates of thrust sheet erosion, and foreland and piggy-back basin formation.

Figure 8 illustrates the effect of crustal-scale thrust faulting and fault-bend fold formation on subsurface temperatures (Husson and Moretti 2002). The steady-state thermal field is shown for variable thrust displacement rates, a basal heat flow of 50 mWm^{-2}, and constant surface temperature of 0 °C. Erosion is not accounted for and the depth to detachment is 30 km below the surface. Although the geometry of thrusts and depth to detachment are often less (~10 km deep) in fold and thrust belts the example shown illustrates how variations in displacement rates and advective heat transfer by thrust faulting influence subsurface temperatures. For example, at very fast displacement rates of 2 m/yr (Fig. 8a) isotherms become inverted across the fault and could result in an inverted metamorphic grade of rocks exposed at the surface later. As the displacement rate decreases so does the curvature of subsurface isotherms across the fault. At displacement rates of 20 and 2.5 mm/yr (Fig. 8b,c) isotherms are not inverted as in Figure 8a although they are still notably curved across the fault indicating that advective heat transfer due to thrust faulting influences subsurface temperatures and could influence the cooling history of thermochronometer samples (see also ter Voorde et al. 2004). Future work in quantifying thrust tectonic thermal processes is needed to investigate the combined influence of faulting, erosion, shear heating, and crustal thickening on thermochronometer cooling histories. Furthermore, the influence of adjacent imbricate and underlying duplex faulting on rock cooling histories is not well understood.

A key concept illustrated by the previous discussion of normal and thrust fault thermal processes is that lateral heat transfer between fault blocks is commonplace and that a 2D or 3D

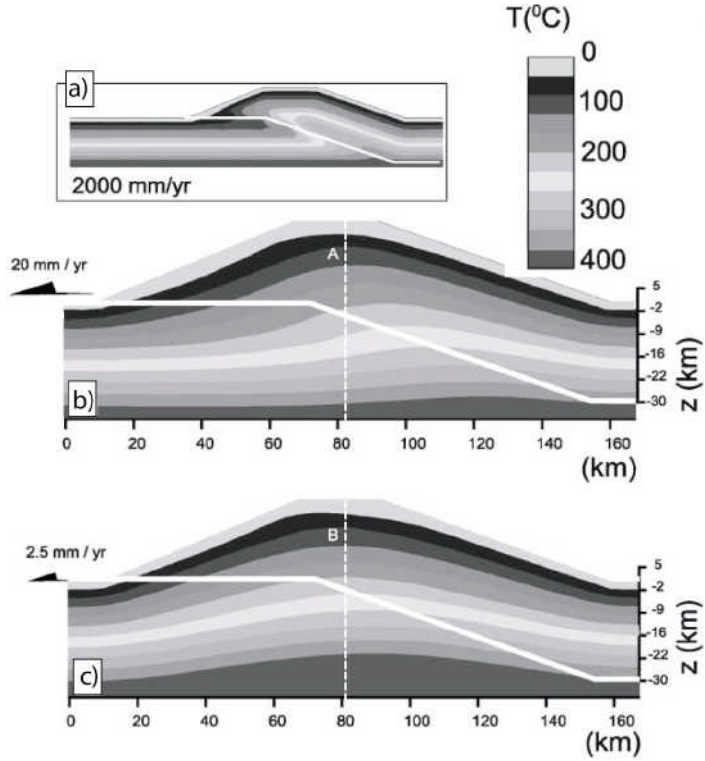

Figure 8. Numerical model predicted sensitivity of steady-state subsurface temperatures to the rate of fault-bend fold formation. (a) Thermal field with a high fault slip rate of 2 m/yr. (b) Thermal field with a fault slip rate of 20 mm/yr. (c) Thermal field with a low fault slip rate of 2.5 mm/yr. Location of fault is shown with solid white line cutting through model. Modified from Husson and Moretti (2002).

representation of the transient thermal field is often needed to make kinematic interpretations out of thermochronometer data. Unfortunately, unlike the previous discussion on the influence of erosion and sedimentation on thermal fields, simple analytic solutions to the advection-diffusion equation are not available in 2D or 3D for realistic fault geometries and inhomogeneous thermal properties of rocks. Thus, numerical solutions (e.g., finite element and finite difference methods) must be applied to quantify thermochronometer cooling history.

Magmatism

The rate of heat loss from magmatic bodies can, in some settings, play an important role in the interpretation of thermochronometer data. High-temperature chronometers (e.g., U/Pb, $^{40}Ar/^{39}Ar$ from hornblende or biotite) collected from within an intrusion often reflect the cooling age of the intrusion and represent the inherited or parent age of a pluton. The parent age of a pluton is useful to know when interpreting low-temperature thermochronometers (e.g., apatite and zircon fission-track or (U-Th)/He methods) that can contain post-emplacement information on the exhumation history of the pluton. Furthermore, the emplacement of magmatic bodies can reheat surrounding country rock to sufficient temperatures to reset low-temperature thermochronometer ages (e.g., Tagami and Shimada 1996, Reiners 2005). Numerous petrologic and heat flow studies have investigated the rate of heat loss from magmatic bodies (e.g., see Furlong et al. 1991; Peacock 1989b for a complementary discussion

and overview). The aim of this section is to summarize previous work and the physics of heat loss around magmatic bodies so that readers have a practical guide to quantifying this process and when it may or may not influence thermochronometer ages.

Heat loss from crustal magmatic bodies primarily occurs through the process of conduction (Philpotts 1990; Spear 1993). Although magmatic bodies have a finite shape the thermal evolution of a magmatic body and its surrounding area can be quantified in 1D with several simplifying assumptions (Peacock 1989a; Furlong et al. 1991; Stuwe 2002). First, the emplacement of magmatic bodies occurs rapidly compared to the post-emplacement thermal equilibration of the surrounding country rock. With this in mind, emplacement can be thought of as occurring instantaneously and solutions to the 1D diffusion equation for a step change in heating can be utilized. Second, the geometry of magmatic bodies are small (typically < 10 km or significantly smaller) relative to the distance to Earth's surface or base of the lithosphere where boundary conditions must be imposed to solve the diffusion equation. Hence, the boundary conditions can be assumed to lie at infinite distance from the intrusion. Finally, the latent heat of fusion from conversion of melt to rock will be neglected to quantify the first-order consequence of magmatism.

Using the previous assumptions, the thermal evolution of an intrusion and the surrounding country rock can be quantified with the 1D transient diffusion equation (Eqn. 2) after removing the heat production term which has negligible influence over the timescales of interest for this problem. Thus, the partial differential equation (Eqn. 2) simplifies to the following form:

$$\alpha \frac{\partial^2 T}{\partial z^2} = \frac{\partial T}{\partial t} \qquad (9)$$

where the variables were previously defined. Equation (9) can be solved for cooling history of a finite width intrusion using the boundary and initial conditions shown in Figure 9. The intrusion is assumed to be planar with width L, and a coordinate system centered in the intrusion and perpendicular to the intrusion walls. Initial conditions used are that at time $t = 0$ the temperature T equals the intrusion temperature T_i within and at the edges of the intrusion $[-(L/2) < z < (L/2)]$ and the temperature T_b equals the background country rock temperature at distances $(L/2) < z < -(L/2)$. Boundary conditions for this problem include the temperature $T = T_b$ at $z = \infty$ and $T = T_i$ at $z = -\infty$ for $t > 0$. With these conditions the solution to Equation (9) is (Carslaw and Jaeger 1959):

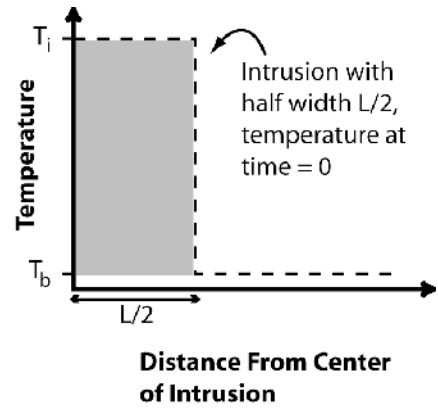

Figure 9. Model setup and initial conditions for 1D thermal model of magmatism (Eqn. 10). Instantaneous intrusion of a body with width L, and intrusion temperature T_i, occurs within country rock with a background temperature T_b.

$$T(z,t) = T_b + \frac{T_i - T_b}{2}\left[erf\left(\frac{L/2 - z}{2\sqrt{\alpha t}}\right) + erf\left(\frac{L/2 + z}{2\sqrt{\alpha t}}\right)\right] \qquad (10)$$

where *erf* is the error function (Abramowitz and Stegun 1970) and z is measured as the distance from the center of the intrusion. Equation (10) can be used to calculate temperatures on each side of the intrusion; however because the boundary and initial conditions imposed

are symmetric around $z = 0$ the solution is also symmetric and only half of the domain need be considered (i.e., from $z = 0$ to $z > 0$).

Figure 10 shows the thermal evolution of intrusions with thicknesses of 100 m, 1 km, and 5 km (Fig. 10a, 10b, 10c, respectively) as well as the thermal evolution of neighboring country rock. An initial intrusion temperature of 700 °C and country rock temperature of 50 °C were chosen to simulate the influence of shallow intrusions on low-temperature thermochronometers in the country rock. A dominant trend in each of the plots is the relaxation, or decrease, in the intrusion temperature and a temporary increase in country rock temperatures. For example,

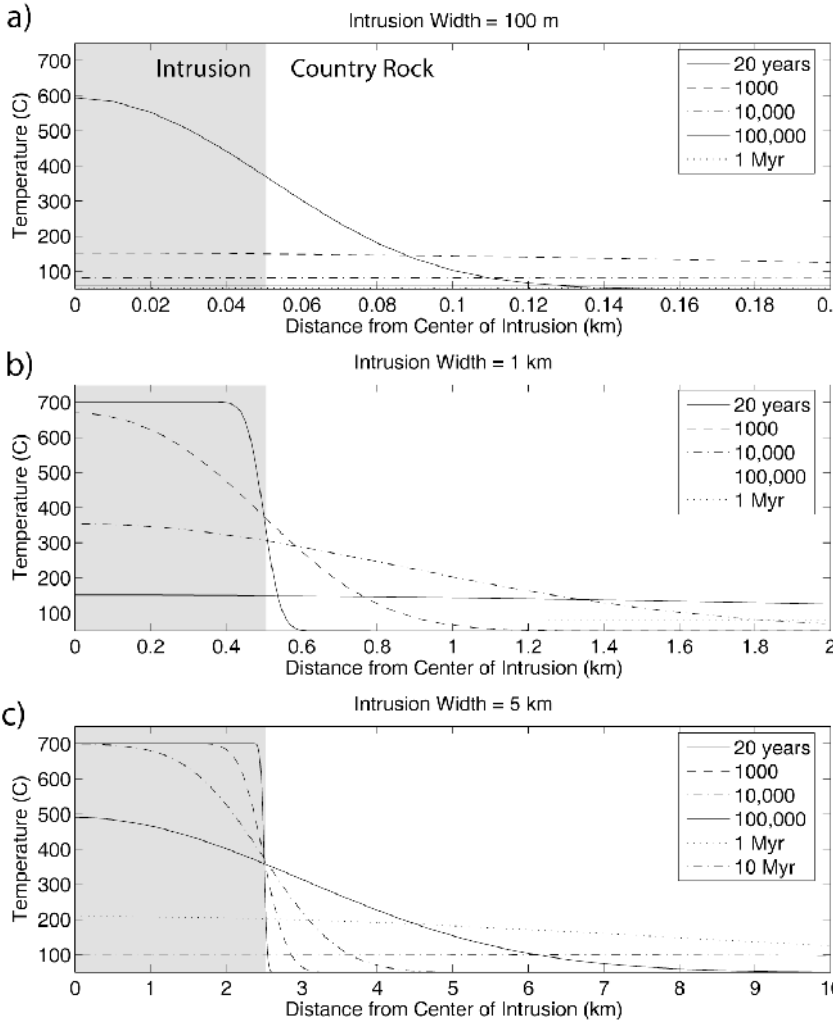

Figure 10. One dimensional transient thermal response to intrusions of various widths. (a), (b), and (c) represent the transient cooling of intrusions and surrounding country rock with intrusion thicknesses of 100 m, 1 km, and 5 km. Temperature profiles were calculated using Equation (10). Intrusion depth was assumed to be shallow and into country rock at background temperature of 50 °C. Other parameters include: initial intrusion temperature of 700 °C, and thermal diffusivity of 32 km^2Ma^{-1}. A Matlab program that reproduces Figure 10 is provided in the supplemental software archive.

with a 1 km wide intrusion (Fig. 10b) between 20 and 1000 years after emplacement of the intrusion the intrusion temperatures decrease from 700 to ~400 °C between the center and wall of the intrusion (0–0.5 km distance). Meanwhile, country rock temperatures (distance > 0.5 km) increase from the background temperature of 50 °C to ~400 °C at the contact and decrease back towards the background temperature at 1 km distance. With increased time since emplacement, temperatures continue to decrease within the intrusion and increase with greater distance from the intrusion. One Ma after emplacement, temperatures are still slightly elevated (~70 °C) above the background temperature between the center of the intrusion and 2 km distance. Thus, the emplacement of intrusions results in a temporary heat pulse that propagates into the country rock and decreases with time.

A second important aspect of Figure 10 is the time required for a heat pulse from an intrusion to decay into the surrounding country rock. The time required for the heat content of an intrusion to dissipate into the surrounding country rock is dependent upon the thermal diffusivity of the rock and the size of the intrusion. A constant thermal conductivity was used in Figure 10 and the discussion here will focus on the effect of intrusion width on the rate of heat dissipation. The smaller the intrusion thickness the faster the temperatures equilibrate back to the background temperature. For example, after 1 Ma with an intrusion thickness of 100 m (Fig. 10a) country rock temperatures (distance > 0.05 km) have equilibrated back to the initial background temperature of 50 °C. However, for an intrusion thicknesses of 5 km (Fig. 10c), 1 Ma after intrusion emplacement country rock temperatures have not equilibrated and are 200–125 °C and decrease with increased distance from the contact. Furthermore, 10 Ma after emplacement (Fig. 10c) country rock temperatures are still elevated to 100 °C. Thus, as intrusion size increases so does the magnitude and duration of heating in adjacent country rock and at greater distances from the intrusion (e.g., Armstrong et al. 1997).

There are several implications of Figure 10 for thermochronometer data collected in country rock adjacent to shallow intrusive bodies. Thermochronometer ages from the country rock will have older, or parent, ages than the intrusion. If samples are collected in the country rock close to the intrusion then the heat pulse associated with intrusion emplacement might reset thermochronometer ages to the intrusion age. Because the magnitude and duration of country rock heating decreases with increased distance from the contact it is possible for thermochronometer ages close to the contact to be reset to the intrusion age whereas samples collected at greater distances will have the parent age of the country rock. Whether or not thermochronometer samples will be reset depends on the magnitude and duration of the heat pulse and the kinetics of He diffusion, Ar loss, and/or fission-track annealing. A detailed analysis of what magnitude and duration of heating is required to reset any given thermochronometer age is beyond the scope of this discussion, and readers should see recent work by Armstrong et al. (1997), Tagami and Shimada (1996) and Reiners (2005). Thus, if the intent of the thermochronometer sampling is to study the magnitude of heating and kinetics of thermochronometer ages then samples should be collected with increasing distance from the intrusion with a finer sampling interval close to the contact. Alternatively, if the objective of a study is to quantify the exhumation history of the country rock then sampling far away from the intrusion is desirable and Equation (10) and Figure 10 can be used to approximate, for different size intrusions, what distance is sufficiently large enough to record cooling associated with country rock exhumation rather than reheating and cooling associated with magmatism.

A thorough study modeling intrusive thermal processes and thermochronometer age responses with distance from the intrusion has not been conducted. Additional work is needed along the lines of (Reiners 2005) to not only measure multiple thermochronometer system ages with increased distance from the intrusion of different sizes and compositions, but also to quantify intrusion thermal processes and evaluate if other associated heat transfer processes

such as hydrothermal fluid flow along intrusion contacts can significantly influence intrusion thermal processes (e.g., Cook and Bowman 2000; Cui et al. 2001).

Topography

The temperature field of the upper crust is sensitive to overlying topography (e.g., Fig. 6). Hence, the cooling history of exhumed thermochronometer samples will vary from point to point beneath topography. Unlike the previous examples (Figs. 7 and 8) in which variations in cooling histories and thermochronometer ages resulted from spatial variability in exhumation rate, here cooling histories and thermochronometer sample age variations can be produced in a region experiencing uniform erosion but beneath topography. The distribution of ages at the surface may thus be inverted for paleotopography to provide important limits on paleoelevation. Several studies have highlighted the utility of apatite (U-Th)/He ages for this approach (e.g., House et al. 1998; House et al. 2001; Persono et al. 2002).

The effect of topography on subsurface temperatures has long been known (Lees 1910), and more recent studies have investigated how topography affects cooling histories using 2D and 3D thermal models (Stuwe et al. 1994; Mancktelow and Grasemann 1997; Braun 2002, 2005; Stuwe 2002; Ehlers and Farley 2003). These studies conclude that spatial and temporal variations in cooling rate depend on the wavelength and amplitude of the topography, as well as the exhumation rate and duration. The implications of topography for low temperature cooling ages in exhuming terrains are not generally appreciated and is an area of active research. For additional information on this topic the reader is referred to a thorough synthesis of recent techniques for quantifying topographic change in a companion chapter in this volume by (Braun 2005).

Fluid flow

The previous discussion of crustal thermal processes emphasized conductive heat transfer in stable cratonal settings and conductive and advective heat transfer due to erosion, sedimentation, and faulting. Fluid flow within the upper crust can also significantly perturb the background conductive thermal state of the crust (e.g., Fig. 3) by advective transport of heat by water. A rich body of literature is available quantifying regional scale fluid flow and thermal processes in sedimentary aquifers (e.g., Smith and Chapman 1983 and references therein). Fluid flow in alpine settings, where thermochronometer data are often collected, is unfortunately less well studied. Furthermore, to date no study has addressed the influence of alpine fluid flow on the interpretation of thermochronometer data in age-elevation plots. The purpose of this section is to highlight the relevant hydrologic and thermal processes controlling alpine fluid flow and to draw the readers attention to how these processes can influence thermochronometer cooling ages in age-elevation plots.

Several quantitative studies have investigated the influence of mountain topography on fluid flow (e.g., Freeze and Witherspoon 1967; Jamieson and Freeze 1983; Toth and Millar 1983; Ingebritsen and Sorey 1985; Forster and Smith 1989). Tell-tale signs of active fluid flow in mountainous settings are warm and hot springs discharging at valley bottoms. Paleosprings can are often indicated by hydrothermally altered rock near fractures. It is important to note that springs are ephemeral features and last on the order of 10^4–10^5 years and change location (Elder 1965). Thus, the present-day distribution and thermal power output from springs is not necessarily a good indicator of ancient fluid flow patterns and careful attention to the field geology is also important.

Mountain fluid and heat flow are related through several processes (Forster and Smith 1988a). In mountainous settings, topography causes lateral variations in pressure that drive fluid flow from range crests to valley bottoms (Fig. 6). This type of flow can be thought of as topographically-driven fluid flow and is often responsible for groundwater discharge into

mountain streams and hot springs (e.g., Ehlers and Chapman 1999; Manning and Solomon 2003). Thus, mountain topography can enhance groundwater circulation to greater depths where temperatures are warmer and the water will capture heat prior to discharge at the surface. Topographically induced lateral temperature variations can influence fluid density and viscosity, thereby altering the rates and patterns of groundwater flow. Thermally induced variations in fluid density can produce a buoyancy-driven vertical fluid flow. Rates of fluid flow can increase from the reduced viscosity of water at higher temperatures. Although elevated subsurface temperatures under mountains can increase rates of fluid flow it is important to note that rocks in mountainous terrains often have significantly lower permeabilities than sedimentary aquifers. Lower permeabilities in mountain settings can result in longer timescales for fluid flow between ridges and valleys (Forster and Smith 1988a). Fluid flow can discharge as hot springs along range fronts if fracture zones associated with range-bounding faults or sedimentary basins have higher permeability than the range.

Figure 11 illustrates how topographically driven fluid flow can influence crustal thermal fields. Meteoric water in the form of rain and snow melt recharges groundwater near the range crest. As the groundwater flows toward the topographic low (basin) it warms and captures heat from the surrounding bedrock. The warm groundwater eventually rises toward the valley floor due to thermal buoyancy and/or higher permeability in the range-bounding fault and basin sediments. Some groundwater can bypass the fault and recharge a basin aquifer or exit as a hot spring further out in the valley. The influence of this groundwater path on the subsurface thermal field is as follows. Downward flowing groundwater in the "zone of heat capture" (Fig. 11) depresses thermal gradients and heat flow over the range crest. Warm water exiting at the hot spring or bypassing the fault to the basin can elevate ground temperatures in those areas, as well as increasing thermal gradients and heat flow. If all the water that enters at the range crest exits at the hot spring then a plot of heat flow normalized by the background heat flow (Fig. 11, top) will have equal area above and below the background heat flow value due to conservation of energy (e.g., Ehlers and Chapman 1999).

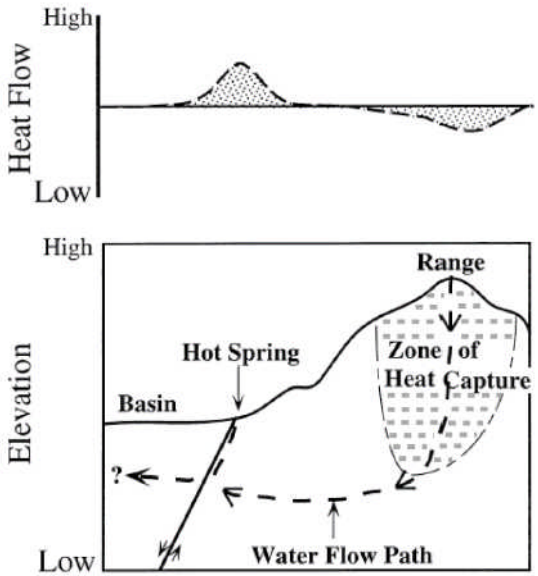

Figure 11. Schematic representation of topographically driven fluid flow and surface heat flow response. Lower panel illustrates groundwater flow paths driven by topography. Heat is captured along the descending path toward the valley and liberated in hot springs or transferred to the adjoining basin. Top panel illustrates how heat flow (and thermal gradients) could be depressed under the range crest and enhanced near the hot spring. Modified from Ehlers and Chapman 1999.

The fluid flow driven depression of thermal gradients under the range crest and elevation of thermal gradients at the valley floor will influence thermochronometer cooling histories of samples collected up the range front. The effect of fluid flow on subsurface temperatures is superimposed upon other relevant thermal processes in this setting, such as topographic, erosional, and faulting effects on subsurface temperatures. Note that although erosion of the range in Figure 11 could enhance thermal gradients, fluid flow could have the opposite effect and depress thermal gradients.

Figure 12 demonstrates the influence of mountain fluid flow on subsurface temperatures. The model accounts for coupled fluid flow and heat transfer for a mountain range with 2 km relief and convex and concave topographic profiles. The models share a common basal heat flow (60 mWm^{-2}), thermal conductivity (2.5 $Wm^{-1}k^{-1}$), impermeable lower and side boundary

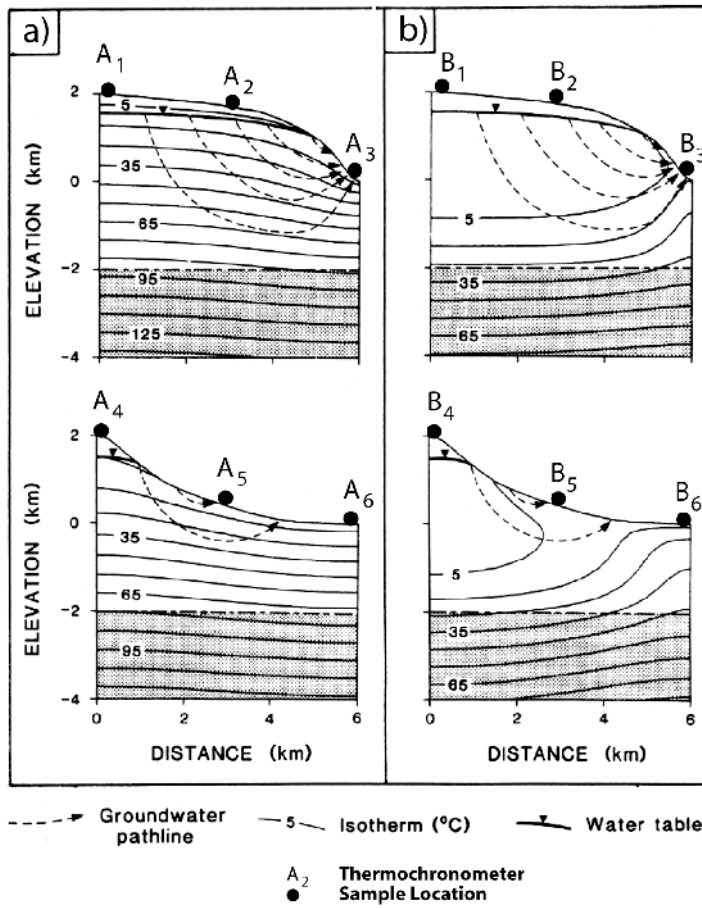

Figure 12. Coupled hydrologic and thermal numerical model results demonstrating the influence of topographically driven fluid flow on subsurface temperatures. See text for model description and parameters. (a) Concave and convex topographic geometries. Fluid flow (dashed lines) is minimal in these simulations, the thermal field is conductive, and not hydrologically disturbed. (b) Same topographies as (a) but thermal field hydrologically disturbed and dominated by advective heat transfer (note change in position of isotherms. Black circles at surface represent hypothetical thermochronometer sample locations discussed in Figure 13. Modified from Forster and Smith (1995).

conditions, and a low-permeability layer below −2 km depth (1.0×10^{-22} m^2). Remaining material properties are described in (Forster and Smith 1988a). The models differ in the permeability of the upper layer above −2 km depth and the infiltration rate at the surface.

The models in Figure 12 demonstrate the transition between conduction and fluid advection dominated thermal fields as a function of increasing permeability in the upper unit. Permeabilities less than 10^{-18} m^2 result in a purely conductive thermal field where shallow isotherms mimic the overlying topography (Fig. 12a). At permeabilities of 10^{-15} m^2 fluid flow significantly perturbs subsurface temperatures and the thermal field is dominated by advective fluid heat transport (Fig. 12b). In a fluid advection dominated thermal field isotherms no longer mimic the overlying topography but rather have a shape that is the inverse of the topography (e.g., compare 35 °C isotherm in Fig. 12a,b). The transition, or threshold, between a conductive and fluid advective thermal field occurs with a permeability around 10^{-16} m^2 (not shown) (Forster and Smith 1988a). The previous threshold permeability corresponds to the lower end of permeabilities associated with rocks present in mountainous settings such as sandstone, limestone and dolomite, and fractured igneous and metamorphic rocks (Freeze and Cherry 1979). The key point illustrated here is that the hydraulic permeability of the upper most crust can have significant influence on subsurface temperatures under certain conditions. Hyrdraulic permeability in mountain settings is controlled not only by lithology but also by secondary fractures generated by removal of overburden and tectonic stresses. A more detailed suite of similar model simulations are presented in (Smith and Chapman 1983; Forster and Smith 1988b,1989).

The transition from a conductive thermal field to one dominated by fluid advection can significantly influence the interpretation of thermochronometer data in age-elevation plots. Figure 12b illustrates how advective heat transport from fluid influences lateral variations in the depth to an assumed closure temperature of 65 °C [e.g., apatite (U-Th)/He closure]. Figure 13 schematically shows how these variations in closure depth could influence ages as a function of elevation. For this thought experiment, uniform erosion of the surface is assumed to occur at a sufficiently low erosion rate (~0.1–0.2 mm/yr) that advective heat transport from erosion is negligible. For a conduction dominated thermal field with concave and convex shaped topography (Fig.12a, filled circles) apatite (U-Th)/He ages will increase with elevation due to the greater distance samples from higher elevations travel from the closure temperature depth (Fig. 13). In this conduction dominated thermal field the samples plot on a straight line. For a fluid advection dominated thermal field with erosion at the same rate as the conductive field the geometry and depth of the 65 °C closure isotherm is perturbed from the conductive field. In the fluid advective model, all samples spend a greater amount of time traveling between the closure temperature and surface and therefore have older ages (Fig. 13, open circles). The increased sample ages in the fluid advective model could be falsely interpreted as exhumation at slower rate when in fact the erosion rate could be the same in both the conductive and fluid advective models. The previous discussion assumes that hydrologic conditions remain constant for the entire time rocks are exhumed.

A second important characteristic of fluid flow on sample ages is that ages do not plot on a straight line as a function of elevation (Fig. 13, open circles). For both topographic geometries considered a concave up curve connects sample ages plotted as a function of elevation. A concave up trend in thermochronometer ages plotted as a function of elevation can also result from a recent change in topographic relief due to differential erosion rates between ridge crests and valley bottoms (Braun 2002). However, in the examples used here a similar concave up trend can occur across topographies with uniform erosion rates and fluid flow between the ridge crest and valley bottom. Thus, caution must be taken when interpreting paleotopography from thermochronometer data that advective heat transport from fluid flow is not biasing the interpretation.

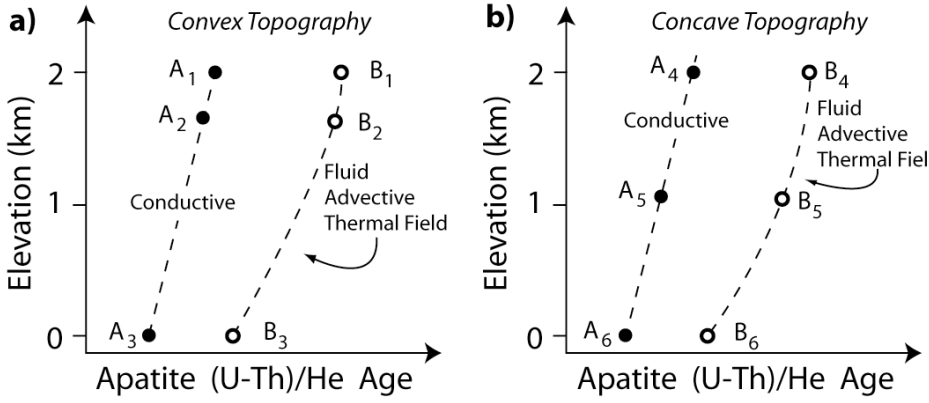

Figure 13. Influence of topographically driven fluid flow on thermochronometer age-elevation plots. (a) Thermochronometer age-elevation relationships for the concave topographies shown in Figure 12. For a conductive (Figure 12a) thermal field (solid circles) thermochronometer samples would plot along a straight line. In an advective fluid flow thermal field (Figure 12b) sample ages would be older (for the same erosion rate as in a conductive simulation) and would have a curved, concave-up geometry that could be falsely interpreted as changing topographic relief. (b) Thermochronometer age-elevation relationships for the convex topographies shown in Figure 12. As with (a) a conductive thermal field produces exhumed sample ages that lie on a straight line. An advective thermal field results in ages that are older and lie along a concave up curve. The relative sample ages shown here were estimated by assuming a constant erosion rate and measuring distances between exhumed sample elevations and the 65 °C isotherms shown in Figure 12.

In summary, the effect of fluid flow on thermochronometer data are as follows: (1) at permeabilities of greater than $\sim 10^{-16}$ m^2 the thermal field can be dominated by fluid advection. (2) all else being equal, fluid dominated thermal fields result in older thermochronometer ages than samples exhumed through a conductive thermal field. Increased thermochronometer ages from fluid flow can result in an overestimate of the timing of the exhumation, and (3) fluid flow can result in a concave up geometry to data plotted as a function of elevation. This concave up pattern could be falsely interpreted as a change in topographic relief. Additional work is needed to quantify the effect of fluid flow on thermochronometer ages. In particular, modeling studies are needed to quantify if fluid flow induced variations in thermochronometer ages significantly influence interpretations of the data when uncertainties in sample age are taken into account. Furthermore, the permeability of mountainous regions with variable fracture density is poorly understood and although the presence or lack of significant fluid flow can be documented with other geochemical or geophysical techniques (e.g., Blackwell et al. 1989; Ehlers and Chapman 1999; Manning and Solomon 2003) studies linking these observations to models that quantify erosion rates and paleotopographic change needs to be conducted.

CONCLUDING REMARKS

This chapter discussed natural variability in crustal thermal gradients and different underlying geologic processes responsible for the observed variability. Mathematic and physical constructs for evaluating thermochronometer thermal histories were presented for the cases of steady-state and transient geotherms, erosion and sedimentation, normal and thrust faulting, magmatism, topography, and hydrothermal fluid flow. In most applications, geologic interpretations of thermochronometer data can be improved by quantifying the thermal consequence of geologic processes responsible for a suite of measured ages. Although thermal modeling of geologic processes is time consuming, the benefits can be rewarding in as much

that additional information (e.g., exhumation rates, fault kinematics, etc.) can be obtained from a data set. Thermal modeling geologic processes prior to collecting samples can provide valuable insight into the magnitude of signal potentially preserved in thermochronometer data as well as the optimal sampling strategy required to capture the predicted signal.

Modeling crustal thermal processes requires careful attention to how different model parameters influence the cooling history. For example, if forward modeling the cooling history in an eroding medium (e.g., Eqn. 7), numerous simulations should be conducted exploring how variations in thermal diffusivity, erosion rate, and erosion duration influence the thermal history of exhumed samples. Predicted thermal histories can be compared to data by calculating cooling rate dependent ages using one of several freely available software packages (e.g., see online software archive). Thus, for each of the tens, hundreds, or thousands of predicted thermal histories, a direct comparison to predicted and observed ages can be made. Statistical comparisons of predicted and observed ages such as a Chi-squared misfit (e.g., Batt et al. 2001; Ehlers et al. 2003, Braun 2005), are efficient ways to identify what combination of model parameters produces the best fit predicted ages to the data.

In an ideal world a perfect and unique model fit to the data will be identified. In reality, individual data points will be outliers to model predicted ages or systematic misfits to the data will be predicted regardless of what combination of model parameters are used. If the later occurs, then the model must be re-evaluated to determine if it is appropriately capturing the relevant thermal processes and additional processes will need to be considered with a different model. Alternatively, several model predicted ages may produce an equally good fit to the data and some uncertainty in the interpretation of the data will be unavoidable.

In many cases, the use of the analytic solutions described here will contain restrictive assumptions (e.g., constant thermal properties, or 1D heat transfer) that require the use of more complicated numerical models to circumvent. The interpretation of geologic events using thermal models and thermochronometer data should be thought of as an iterative process that may take significant effort. The Earth is a complicated environment and multiple combinations of model parameters may produce an equally good fit to the data. Thus, the approach taken should not be to find *the* solution that satisfies the data but rather *the range* of solutions that provide a good fit to the data. The pay-off from the time invested in forward modeling thermal histories is a rigorous and quantitative understanding of the underlying geologic processes responsible for an observed data set.

As a summary to the topics covered in this chapter, the following generalized steps are suggested as guidelines for quantifying the influence of crustal thermal processes on thermochronometer sample collection and interpretation:

Step 1: Compile available surface heat-flow determinations to determine spatial variation in the present day thermal field (e.g., Fig. 1) across the study area. This step is primarily relevant for interpreting samples collected from an active orogenic or magmatic setting and is less relevant for the study of ancient (e.g., Paleozoic) mountain belts. Surface heat-flow determinations should be used to help constrain predicted subsurface temperatures and surface heat flow calculated in steps 3 and 4.

Step 2: Compile relevant thermo-physical properties (e.g., thermal conductivity, heat production, etc) for lithologies present in the study area. Ideally material properties are measured on rocks from within a study region because the range values for any given rock type can sometimes be large (e.g., Appendix A). If measured values from the study area are not possible then table 'lookup' values such as those in appendix A provide a good starting point.

Step 3: Identify the dominant thermal processes influencing thermochronometer thermal histories and quantify the spatial dimensions over which these processes are

relevant. This step requires application of the relevant differential equation(s) for heat transfer discussed in this chapter, or in referenced material. A step-wise increase is model complexity is recommended by starting with simpler 1D equations and increasing to 2D and 3D formulations if needed. The test of whether 1D, 2D, or 3D models are sufficient hinges on the dominant direction(s) of heat flow in the study over the time span that samples cooled. For example, if heat flow is believed to be predominantly vertical then a 1D simulation of heat transfer is sufficient. Alternatively, if significant lateral heat flow occurs in association with samples collected close to active structures (e.g., Ehlers et al. 2003) or long-wavelength topography (e.g., Stuwe et al. 1994; Braun 2002; Ehlers and Farley 2003) then 2D or 3D models should be applied.

Step 4: Quantify if temporal changes in the crustal thermal field influenced the sample thermal history. An important concept illustrated earlier in this chapter (e.g., Figs. 3, 4, 5, 10) is characterization of if the thermal field was in steady state or evolving at the time samples cooled. Various 1D equations and figures in this chapter were presented for determination of the time scales over which subsurface temperatures evolve in magmatic, or erosional and depositional settings (see also Mancktelow and Grasemann 1997). If the thermal field is determined to be transient then some form of the time-dependent diffusion equation should be applied for sample interpretation.

Step 5: After the spatial and temporal variability in the thermal field is characterized then the relevant governing equation should be used to forward model sample cooling histories. These predicted thermal histories can then be used to compute predicted thermochronometer ages, track length distributions, etc, using the thermal histories generated from steps 2 to 4 (see Dunai 2005; Harrison et al. 2005; Ketcham 2005 for a detailed discussions) that can then be compared to the data.

Step 6: Quantify the range of plausible material properties, boundary conditions, and model free parameters that minimize differences between predicted and observed thermal histories and/or thermochronometer ages. This final step requires identification and exploration of all free parameters within the model being used and iteratively applying the model (e.g., step 5) to compare predicted and observed ages and thermal histories. A statistical comparison between model predicted and observed ages and thermal histories is recommended to identify the range of plausible geologic processes that could have produced the observed sample ages and thermal histories.

Unfortunately, every data set and geologic setting requires a different treatment and thermal modeling analysis for a robust interpretation of thermochronometer data. The previous steps are provided mainly as guidelines for assessing the influence of crustal thermal processes on thermochronometer data and additional, or fewer, steps may be required depending on the problem addressed.

ACKNOWLEDGMENTS

This chapter benefited from discussions with the Surface Processes Research Group, Jason Barnes, and other curious graduate students at the University of Michigan. Phillip Armstrong and Kevin Furlong are thanked for thorough and constructed reviews. This chapter resulted from US National Science Foundation funding to the author (EAR 0409289, 0309779, and 0196414).

REFERENCES

Abramowitz M, Stegun I (eds) (1970) Handbook of Mathematical Functions. Dover Publications, New York
Allmendinger R, Shaw J (2000) Estimation of fault propagation distance from fold shape; implications for earthquake hazard assessment. Geology 28(12):1099-1102
Angevine CL, Turcotte DL (1983) Oil generation in overthrust belts. AAPG Bulletin 67:235-241
Armstrong P, Ehlers T, Chapman D, Farley K, Kamp P (2003) Exhumation of the central Wasatch Mountains, Utah: 1. Patterns and timing of exhumation deduced from low-temperature thermochronology data. J Geophys Res 108(3):2172, doi:10.1029/2001JB001708
Armstrong PA, Chapman DS (1999) Beyond surface heat flow: An example from a tectonically active sedimentary basin. Geology 26:183-186
Armstrong PA, Kamp PJ, Allis RG, Chapman DS (1997) Timing of the heat flow high on Taranaki Peninsula (New Zealand): evidence from combined apatite fission track age and vitrinite reflectance data. Basin Res 9:151-169
Batt G, Brandon M, Farley K, Roden-Tice M (2001) Tectonic synthesis of the Olympic Mountains segment of the Cascadia wedge, using two-dimensional thermal and kinematic modeling of thermochronological ages. J Geophys Res 106(B11):26731-26746
Benfield A (1949a) The effect of uplift and denudation on underground temperatures. J Appl Phys 20:66-70
Benfield A (1949b) A problem of the temperature distribution in a moving medium. Quart Appl Math 6:439-443
Bertotti G, Seward D, Wijbrans J, ter Voorde M, Hurford A (1999) Crustal thermal regime prior to, during, and after rifting; a geochronological modeling study of the Mesozoic South Alpine rifted margin. Tectonics 18(2):185-200
Bertotti G, ter Voorde M (1994) Thermal effects of normal faulting during rifted basin formation; 2, The Lugano-Val Grande normal fault and the role of pre-existing thermal anomalies. Tectonophysics 240(1-4):145-157
Blackwell DD, Steele JL, Wisian KW (1994), Results of geothermal resource evaluation for the eastern United States. Geothermal Resources Council Trans 18:161-164
Blackwell DD, Wisian KW, Richards M (1996) Geothermal resources of the United States based on heat flow and gradient information, DOE Report Contract #C91-103450
Blackwell D, Steele J, Brott C (1989) Heat flow in the Pacific Northwest. *In:* Physical Properties of Rocks and Minerals. Touloukian Y, Judd W, Roy R (eds) McGraw-Hill, New York, p 495-502
Boyer S, Elliot D (1982) Thrust systems. AAPG Bulletin 66(9):1196-1230
Braun J (2002) Quantifying the effect of Recent relief changes on age-elevation relationships. Earth Planet Sci Lett 200(3-4):331-343
Braun J (2005) Quantitative constraints on the rate of landform evolution derived from low-temperature thermochrohonology. Rev Mineral Geochem 58:351-374
Brewer J (1981) Thermal effects of thrust faulting. Earth Planet Sci Lett 56:233-244
Burtner R, Nigrini A (1994) Thermochronology of the Idaho-Wyoming thrust belt during the Sevier Orogeny; a new, calibrated, multiprocess thermal model. AAPG Bulletin 78(10):1586-1612
Burtner R, Nigrini A, Donelick R (1994) Thermochronology of lower Cretaceous source rocks in the Idaho-Wyoming thrust belt. AAPG Bulletin 78(10):1613-1636
Carslaw H, Jaeger J (1959) Conduction of Heat in Solids. Clarendon Press, Oxford
Cermak V, Rybach L (1982) Thermal conductivity and specific heat of minerals and rocks. *In:* Landolt-Bornstein Numerical Data and Functional Relationships in Science and Technology, New Series, Group V. Angenheister G (ed), Springer-Verlag, Berlin, p. 89-134
Cerveny PF, Steidtmann JR (1993) Fission track thermochronology of the Wind River Range, Wyoming; evidence for timing and magnitude of Laramide exhumation. Tectonics 12(1):77-92
Chapman D (1986) Thermal gradients in the continental crust. Geol Soc Spec Publ 24:63-70
Chapman D, Pollack H (1975) Global heat flow: a new look. Earth Planet Sci Lett 28:23-32
Chapman D, Rybach L (1985) Heat flow anomalies and their interpretation. J Geodynamics 4(1-4):3-37
Chapman DS, Furlong KP (1992) The thermal state of the lower crust, in continental lower crust. *In:* Development in Geotectonics. Volume 23. Fountain DM, Arculus RJ, Kay RM (eds) Elsevier, Amsterdam, p 179-199
Clark S (1966) Handbook of Physcial Constants. Memoir Geological Society of America, 97. Geological Society of America, New York
Commision IHF (2004) Global heat flow data base. *http://www.heatflow.und.edu/index2.html*
Condon EU, Odishaw H (1967) Handbook of Physics. McGraw-Hill, New York
Cook SJ, Bowman JR (2000) Contact metamorphism surrounding the Alta stock fluid rock interaction accompanying metamorphism of siliceous dolomites. J Petrology 41:739-757

Cui X, Nabelek PI, Liu M (2001) Controls of layered and transient permeability on fluid flow and thermal structure in contact metamorphic aureals, with application to the Notch Peak aureole, Utah. J Geophys Res 106:6477-6491

Dahlstrom CDA (1969) Balanced cross sections. Can J Earth Sci 6:743-757

Davy P, Gillett P (1986) The stacking of thrust slices in collision zones and its thermal consequences. Tectonics 5:913-929

Dodson MH (1973) Closure temperature in cooing geochronological and petrological systems. Contrib Mineral Petrol 40:259-274

Dodson MH (ed) (1986) Closure Profiles in Cooling Systems. Materials Science Forum, 7. Trans Tech Publications, Aedermannsdorf, Switzerland, 145-153 pp

Dunai TJ (2005) Forward modeling and interpretation of (U-Th)/He ages. Rev Mineral Geochem 58:259-274

Edman JD, Furlong KP (1987) Thrust faulting and hydrocarbon generation: A reply. AAPG Bulletin 71:890-896

Edman JD, Surdam RC (1984) Influence of overthrusting on maturation of hydrocarbons in Phosphoria Formation, Wayoming-Idaho-Utah overthrust belt. AAPG Bulletin 68:1803-1817

Ehlers T, Chapman D (1999) Normal fault thermal regimes; conductive and hydrothermal heat transfer surrounding the Wasatch Fault, Utah. Tectonophysics 312(2-4):217-234

Ehlers T, Farley K (2003) Apatite (U-Th)/He thermochronometry; methods and applications to problems in tectonic and surface processes. Earth Planet Sci Lett 206(1-2):1-14

Ehlers TA, Armstrong PA, Chapman D (2001) Normal fault thermal regimes and the interpretation of low-temperature thermochronometers. Phys Earth Planet Interiors 126:179-194

Ehlers TA, Willett SD, Armstrong PA, Chapman DS (2003) Exhumation of the central Wasatch Mountains, Utah: 2. Thermokinematic model of exhumation, erosion, and thermochronometer interpretation. J Geophys Res 108(B3):2173, doi:10.1029/2001JB001723

Elder J (ed) (1965) Physcial Processes in Geothermal Areas. Terrestrial Heat Flow, Geophysical Monograph 8. American Geophysical Union, Washington D.C.

Elliott D (1976) The energy balance and deformation mechanisms of thrust sheets. Phil Trans Royal Soc London 283:289-312

Elliott D (1977) Some aspects of the geometry and mechanics of thrust belts, Parts 1 and 2. 8th Annual Seminar Canadian Society of Petroleum Geology. University of Calgary, Calgary

Elliott D (1983) The construction of balanced cross-sections. J Struct Geol 5:101-126

England PC, Molnar P (1993) The interpretation of inverted metamorphic isograds using simple physical calculations. Tectonics 12:145-158

England PC, Thompson AB (1984) Pressure-Temperature-time paths of regional metamorphism I. Heat transfer during the evolution of regions of thickened continental crust. J Petrology 25:894-928

Farley K (2000) Helium diffusion from apatite; general behavior as illustrated by Durango fluorapatite. J Geophys Res 105(B2):2903-2914

Forster C, Smith L (1988a) Groundwater flow systems in mountainous terrain; 1, Numerical modeling technique. Water Resour Res 24(7):999-1010

Forster C, Smith L (1988b) Groundwater flow systems in mountainous terrain; 2, Controlling factors. Water Resour Res 24(7):1011-1023

Forster C, Smith L (1989) The influence of groundwater flow on thermal regimes in mountainous terrain: a model study. J Geophys Res 94(B7):9439-9451

Freeze AR, Cherry JA (1979) Groundwater. Prentice Hall, Englewood Cliffs, NJ

Freeze RA, Witherspoon PA (1967) Theoretical analysis of regional groundwater flow, 2. Effect of water table configuration and subsurface permeability variations. Water Resour Res 3:623-634

Furlong K, Chapman D (1987) Crustal heterogeneities and the thermal structure of the continental crust. Geophys Res Lett 14(3):314-317

Furlong KP, Edman JD (1984) Graphical approach to the determination of hydrocarbon maturation in overthrust terrains. AAPG Bulletin 68:1818-1824

Furlong KP, Edman JD (1989) Hydrocarbon maturation in thrust belts; thermal considerations. *In:* Origin and Evolution of Sedimentary Basins and Their Energy and Mineral Resources. Geophysical Monograph, vol. 48, IUGG vol. 3. Price RA (ed) American Geophysical Union, Washington, DC, p 137-144

Furlong KP, Hanson RB, Bowers JB (1991) Modeling thermal regimes. Rev Mineral 26:437-506

Furlong KP, Londe MD (eds) (1986) Thermal-mechanical consequences of basin and range extension. *In:* Extensional Tectonics of the Basin and Range Province: A Perspective. GSA Special Paper 208. Mayer L (ed) Geological Society of America, Boulder, p 23-30

Govers R, Wortel M (1995) Extension of stable continental lithosphere and the initiation of lithosphere scale faults. Tectonics 14(4):1041-1055

Graham CM, England PC (1976) Thermal regimes and regional metamorphism in the vicinity of overthrust faults: an example of shear heating and inverted metamorphic zonation from southern California. Earth Planet Sci Lett 31:142-152
Haenel R, Rybach L, Stegena L (1988) Handbook of Terrestrial Heat-flow Density Determination; with guidelines and recommendations of the international Heat Flow Commission. Kluwer-Acad., Dordrecht
Harrison TM, Grove M, Lovera OM, Zeitler PK (2005) Continuous thermal histories from inversion of closure profiles. Rev Mineral Geochem 58:389-409
Homza TX, Wallace WK (1995) Geometric and kinematic models for detachment folds with fixed and variable detachment depths. J Struct Geol 17:575-588
House M, Wernicke B, Farley K (1998) Dating topography of the Sierra Nevada, California, using apatite (U-Th)/He ages. Nature 396(6706):66-69
House MA, Wernickey KA, Farley KA (2001) Paleo-geomorphology of the Sierra Nevada, California, from (U-Th)/He ages in apatite. Am J Sci 301:77-102
Husson L, Moretti I (2002) Thermal regime of fold and thrust belts - an application to the Bolivian sub Andean zone. Tectonophysics 345:253-280
Ingebritsen SE, Sorey ML (1985) A quantitative analysis of the Lassen hydrothermal system, North Central California. Water Resour Res 21:853-868
Jamieson GR, Freeze RA (1983) Determining hydraulic conductivity distribution in a mountainous area using mathematical modeling. Groundwater 21:168-177
Jones PB (1971) Folded faults and sequences of thrusting in Alberta foothills. AAPG Bulletin 55:292-306
Kappelmeyer O, Haenel R (1974) Geothermics, with Special Reference to Application. Gebruder Borntraeger, Berlin
Karabinos P, Ketcham R (1988) Thermal Structure of Active Thrust Belts. J Metamorph Geol 6(5):559-570
Ketcham RA (2005) Forward and inverse modeling of low-temperature thermochronometry data. Rev Mineral Geochem 58:275-314
Lachenbruch A (1968) Rapid estimation of the topographic disturbance to superficial thermal gradients. Rev Geophys 6(3):365-400
Lachenbruch A, Sass J (1978) Models of an extending lithosphere and heat flow in the Basin and Range Province. GSA Memoir 152:209-250
Lachenbruch A, Sass J (1980) Heat flow and energetics of the San Andreas fault zone. J Geophys Res 85(B11): 6185-6222
Lee Y, Deming D (1999) Heat flow and thermal history of the Anadarko Basin and the western Oklahoma platform. Tectonophysics 313(4):399-410
Lees CH (1910) On the isogeotherms under mountain ranges in radioactive districts. Proc Royal Soc 83:339-346
Mailhe D, Lucazeau F, Vasseur G (1986) Uplift history of thrust belts; an approach based on fission track data and thermal modelization. Tectonophysics 124(1-2):177-191
Mancktelow N, Grasemann B (1997) Time-dependent effects of heat advection and topography on cooling histories during erosion. Tectonophysics 270(3-4):167-195
Manning A, Solomon D (2003) Using noble gases to investigate mountain-front recharge. J Hydrology 275(3-4):194-207
Martel SJ (1999) Mechanical controls on fault geometry. J Struct Geol 21:585-596
Mitra S (1986) Duplex structures and imbricate thrust systems; geometry, structural position, and hydrocarbon potential. AAPG Bulletin 70(9):1087-1112
Molnar P, England PC (1990) Temperatures, heat flux, and frictional stress near major thrust faults. J Geophys Res 95:4833-4856
Omar GI, Lutz TM, Giegengack R (1994) Apatite fission-track evidence for Laramide and post-Laramide uplift and anomalous thermal regime at the Beartooth overthrust, Montana-Wyoming. Geol Soc Am Bull 106(1):74-85
O'Sullivan PB, Wallace WK, Murphy JM (1998) Fission-track evidence for apparent out-of-sequence Cenozoic deformation along the Philip Smith Mountain Front, northeastern Brooks Range, Alaska. Earth Planet Sci Lett 164(3-4):435-449
Oxburgh ER, Turcotte DL (1974) Thermal gradients and regional metamorphism in overthrust terrains with special reference to the Eastern Alps. Schweiz Mineral. Petrogra Mitt 54:641-662
Peacock SM (1989a) Numerical constraints on rates of metamorphism, fluid production, and fluid flux during regional metamorphism. Geol Soc Am Bull 101:476-485
Peacock SM (1989b) Thermal modeling of metamorphic P-T-t paths. *In:* Metamorphic P-T-t Paths. Spear FS, Peacock SM (eds), American Geophysical Union, p 57-102
Persono C, Stuart F, Bishop P, Barfod D (2002) Apatite (U-Th)/He age constraints on the development of the Great Escarpment on the southeastern Australian passive margin. Earth Planet Sci Lett 200:79-90
Philpotts AR (1990) Principles of Igneous and Metamorphic Petrology. Prentice Hall, Englewood Cliffs

Platt JP, Leggett JK, Young J, Raza H, Alam S (1985) Large-scale sediment underplating in the Makran accretionary prism, southwest Pakistan. Geology 13:507-511
Pollack H (1982) The heat flow from the continents. Annual Rev Earth Planet Sci 10:459-481
Pollack H, Chapman D (1977) On the regional variation of heat flow, geotherms, and lithospheric thickness. Tectonophysics 38(3-4):279-296
Pollack H, Hurter S, Johnson J (1993) Heat flow from the Earth's interior; analysis of the global data set. Rev Geophys 31(3):267-280
Popov Y, Pribnow D, Sass J, Williams C, Burkhardt H (1999) Characterization of rock thermal conductivity by high-resolution optical scanning. Geothermics 28:253-276
Powell W, Chapman D, Balling N, Beck AE (1988) Continental heat-flow density. *In:* Handbook of Terrestrial Heat-Flow Density Determination. Haenel R, Rybach L, Stegena L (eds), Kluwer Academic Publishers, Dordrecht p 167-222
Pribnow D, Sass J (1995) Determination of thermal conductivity for deep boreholes. J Geophys Res 100(B6): 9981-9994
Quidelleur X, Grove M, Lovera O, Harrison T, Yin A (1997) Thermal evolution and slip history of the Renbu Zedong Thrust, southeastern Tibet. J Geophys Res 102(B2):2659-2679
Rahn M, Grasemann B (1999) Fission track and numerical thermal modeling of differential exhumation of the Glarus thrust plane (Switzerland). Earth Planet Sci Lett 169(3-4):245-259
Reiners PW (2005) Zircon (U-Th)/He thermochronometry. Rev Mineral Geochem 58:151-179
Roy R, Beck A, Touloukian Y (1981) Thermo-physical properties of rocks. *In:* Physical Properties of Rocks and Minerals. Touloukian Y, Judd W,Roy R (eds), McGraw-Hill, New York, p 409-502
Ruppel C, Hodges K (1994) Role of horizontal thermal conduction and finite time thrust emplacement in simulation of pressure-temperature-time paths. Earth Planet Sci Lett 123(1-4):49-60
Ruppel C, Royden L, Hodges K (1988) Thermal modeling of extensional tectonics; application to pressure-temperature-time histories of metamorphic rocks. Tectonics 7(5):947-957
Ryback L, Cermak V (1982) Radioactive heat generation in rocks. *In:* Landolt-Bornstein Numerical Data and Functional Relationships in Science and Technology, Group V. Angenheister G (ed), Springer-Verlang, Berlin, pp. 353-371
Salvini F, Storti F, McClay K (2001) Self-determining numerical modeling of compressional fault-bend folding. Geology 29(9):839-842
Sass JH, Blackwell DD, Chapman DS, Costain JK, Decker ER, Lawyer LA, Swanberg CA, Blackstone DL, Brott CA, Heasier HP, Lachenbruch AH, Marshall BV, Morgan PM, Robert J, Steele JL (1981) Heat flow from the crust of the United States. *In:* Physical Properties of Rocks and Minerals. Touloukian Y, Judd W, Roy R (eds), McGraw-Hill, New York, p 503-548
Shi Y, Wang C (1987) Two-dimensional modeling of the P-T-t paths of regional metamorphism in simple overthrust terrains. Geology 15(11):1048-1051
Shuster DL, Farley KA (2005) $^{4}He/^{3}He$ thermochronometry: theory, practice, and potential complications. Rev Mineral Geochem 58:181-203
Smith L, Chapman D (1983) On the thermal effects of groundwater flow; 1. regional scale systems. J Geophys Res 88(B1):593-608
Somerton WH (1992) Thermal Properties and Temperature-related Behavior of Rock/Fluid Systems. Developments in petroleum science, 37. Elsevier, Amsterdam
Spear FS (1993) Metamorphic Phase Equilibria and Pressure-Temperature-Time Paths. Mineralogical Society of America, Washington D.C.
Stock J, Montgomery D (1996) Estimating palaeorelief from detrital mineral age ranges. Basin Res 8(3): 317-327
Stuwe K (2002) Introduction to the Geodynamics of the Lithosphere: Quantative Description of Geological Problems. Springer-Verlag, Berlin
Stuwe K, White L, Brown R (1994) The influence of eroding topography on steady-state isotherms; application to fission track analysis. Earth Planet Sci Lett 124(1-4):63-74
Suppe J (1976) Decollement folding in southwestern Taiwan. Pet Geol Taiwan 13:25-35
Suppe J (1980) Imbricated structure of Western Foothills Belt, southcentral Taiwan. Pet Geol Taiwan 17:1-16
Suppe J (1983) Geometry and kinematics of fault-bend folding. Am J Sci 283(7):684-721
Tagami T, Shimada C (1996) Natural long-term annealing of the zircon fission track system around a granitic pluton. J Geophys Res 101(4):8245-8255
Taylor S, McLennan S (1981) The composition and evolution of the continental crust: rare earth element evidence from sedimentary rocks. Phil Trans Royal Soc London 301:381-399
ter Voorde M, Bertotti G (1994) Thermal effects of normal faulting during rifted basin formation. 1. A finite difference model. Tectonophysics 240:133-144

ter Voorde M, de Bruijne CH, Cloetingh SAPL, Andriessen PAM (2004) Thermal consequences of thrust faulting: simultaneous versus successive fault activation and exhumation. Earth Planet Sci Lett 223: 395-413

Thorbjornsen KL, Dunne WM (1997) Origin of a thrust-related fold: geometric vs kinematic tests. J Struct Geol 19:309-319

Toth J, Millar R (1983) Possible effects of erosional changes of the topographic relief on pore pressures at depth. Water Resour Res 19(6):1585-1597

Touloukian YS, Judd WR, Roy RF (eds) (1989) Physical Properties of Rocks and Minerals. CINDAS data series on material properties, Group II, Properties of special materials, II-2. McGraw-Hill, New York

van Wees J, de Jong K, Cloetingh S (1992) Two-dimensional P-T-t modelling and the dynamics of extension and inversion in the Betic Zone (SE Spain). Tectonophysics 203(1-4):305-324

APPENDIX A: THERMOPHYSICAL PROPERTIES OF EARTH MATERIALS

The appendix tables contain compilations of thermophysical properties for common geologic materials. These tables are provided to give readers an appreciation for the natural variability, and average values, of thermal conductivity (Table A1), specific heat (Table A2), and volumetric radiogenic heat production (Table A3). The values presented here can be used for forward modeling crustal thermal properties using equations presented earlier.

Table A1. Thermal conductivity of common geologic materials.

Material Type	*Mean Value* W/m°K	*Range of values* W/m°K	*# of Samples*	*Ref.*	*Comments*
Unconsolidated Material and Water					
Clay/Mud	2.1	1.7-3.2	na	[3]	At least 40% saturated
Soil	0.69	0.4-0.9	na	[3]	Saturated
	3.9	2.1-5.3	na	[3]	Unsaturated
Water	1.4	na	na	[4]	At 0 °C
Sedimentary Rocks					
Sandstone	4.7	3.5-7.7	7	[3]	
Limestone	3.3	1.3-6.26	445	[1]	
Shale	2.48	1.00-3.96	na	[2]	
	3.88	2.8-5.6	31	[3]	
Sandstone+Shale	1.67	na	223	[6]	*In situ* Measurements
Limestone+Shale	2.08	1.90-2.61	385	[6]	*In situ* Measurements
Limestone+Sandstone+Shale	2.55	na	44	[6]	*In situ* Measurements
Igneous Rocks					
Granite	3.3	1.78-5.02	130	[1]	
	7.8	6.2-9.0	12	[3],[4]	High quartz content
Rhyolite	1.3	0.92-1.68	na	[3]	
Basalt	1.7	1.12-2.38	72	[1]	
	1.8	1.6-2.0	na	[2]	
	4	na	na	[4]	
Gabbro	5.6	na	na	[3]	At 0 °C
Metamorphic Rocks					
Gneiss	2.95	1.7-5.8	379	[1]	
	6.58	4.6-8.0	37	[3]	High quartz content
	3.49	3.7-3.5	54	[5]	
	3.38	1.9-4.6	30	[7]	
Schist	3.6	2.1-4.6	96	[1]	
	6.6	4.1-8.9	15	[3]	High quartz content
Marble	2.8	2.02-5.59	218	[1], [4]	
Amphibolite	3.4	1.8-4.7	66	[1]	
	2.5	na	27	[5]	
	2.6	2.4-2.8	6	[7]	

Notes: All measurements made at ~20°C unless stated, na = information not available

References: [1] Touloukian et al. 1989; [2] Somerton 1992; [3] Clark 1966; [4] Condon and Odishaw 1967; [5] Pribnow and Sass 1995; [6] Lee and Deming 1999; [7] Popov et al. 1999

Table A2. Specific heat of common geologic materials.

Material Type	*Mean Value* J/kg°K	*Range of values* J/kg°K	*Ref.*
Soil, Air, Water			
Air	1006	na	[2]
Soil	922	796-1005	[2]
Water	4190	na	[2]
Sedimentary Rocks			
Sandstone	964	na	[2]
Limestone	860	910-810	[1]
Igneous Rocks			
Granite	880	na	[1]
Basalt	788	700-875	[1]
Gabbro	775	835-715	[1]
Metamorphic Rocks			
Marble	883	903-863	[1]

Notes: All measurements made at ~20 C; na = information not available
References: [1] Touloukian et al. 1989; [2] Carslaw and Jaeger 1959

Table A3. Volumetric radiogenic heat production of common geologic materials.

Material Type	*Mean Value* $\mu W/m^3$	*Range of values* $\mu W/m^3$	*Ref.*
Sedimentary Rocks			
Sandstone	0.66	0.32-0.99	[1]
Limestone	0.62	na	[1]
Shale	1.80	1.8-5.5	[1]
Igneous Rocks			
Granite	2.45	na	[1]
Dacite	1.48	na	[1]
Diorite	1.08	na	[1]
Basalt	0.31	na	[1]
Gabbro	0.31	na	[1]

Notes: na = information not available
Reference = [1] Haenel et al. 1988